COMPUTATIONAL MODEL FOR STEADY STATE SIMULATION OF A PLATE-FIN HEAT EXCHANGER

by

AJIT RAJESH DESAI

Presented to the Faculty of the Graduate School of

The University of Texas at Arlington in Partial Fulfillment

of the Requirements

for the Degree of

MASTER OF SCIENCE IN MECHANICAL ENGINEERING

THE UNIVERSITY OF TEXAS AT ARLINGTON

DECEMBER 2015

ACKNOWLEDGEMENTS

I sincerely thank my supervising professor Dr. Daejong Kim for giving guidance and support for my career development. Dr. Kim's expertise in his field of work will always be a source of inspiration for me. I am grateful to him, since he gave me the opportunity to work at Turbomachinery and Energy Systems Laboratory and elevate my knowledge and capabilities. I would like to specially thank Dr. Hyejin Moon and Dr. Ratan Kumar for their time and effort in being a part of my thesis committee.

I would like to thank Behzad Yajdi, Sandeep Patil, Srikant, Dr. Xu and my colleagues at Turbomachinery and Energy Systems Laboratory, for all the support and guidance. My skills would not have been the same without their help. I thank my parents for their love, and for believing in me and my objectives.

November 23, 2015

ABSTRACT

COMPUTATIONAL MODEL FOR STEADY STATE SIMULATION OF A PLATE-FIN HEAT EXCHANGER

Ajit Rajesh Desai, M.S.

The University of Texas at Arlington, 2015

Supervising Professor: Daejong Kim

High performance heat transfer devices are critical components in hybrid power generation systems. The design of a Recuperator for ‘waste heat recovery’ is crucial for reducing the operating cost of a hybrid system. Plate-fin heat exchangers occupy a special position among high performance heat exchangers because of the compactness, efficiency and flexibility they offer. The performance of these heat exchange devices is typically very sensitive to fluid property variations, axial conduction and heat losses to environment.

This thesis presents a numerical model of a plate fin heat exchanger in which fluid property variations including temperature driven changes in specific heat capacity, viscosity and heat transfer coefficients, and axial conduction effects are explicitly modeled. The objective is to predict fluid properties at outlet of the heat exchanger as accurately as possible, using a computationally less expensive procedure. Finite Volume Method is used for discretization of the domain. Momentum equation is modelled using flow admittance concept and energy transport across flow field is modeled using the Advection-Diffusion equation. The model solves for mass flow rate and temperatures of fluid streams and for temperatures of solid structure. The numerical model is validated

against analytical solutions in the appropriate limits and then used to analyze performance of an example heat exchanger core under specific set of operating conditions prescribed by a Solid Oxide Fuel Cell-Gas Turbine hybrid system cycle, in order to demonstrate its utility.

The resulting numerical model is simple to implement and computationally efficient, therefore it can be easily integrated into complex system models as a sub-routine and also can be used as a stand-alone solver for parallel-flow or counter-flow heat exchanger simulation.

TABLE OF CONTENTS

LIST OF ILLUSTRATIONS

LIST OF TABLES

Chapter 1

INTRODUCTION

1.1 Background

The increasing energy demands, limited fossil fuel resources and environmental concerns have caused researchers in power generation technology field to focus their attention on increasing efficiency and reducing emissions. Distributed power generation refers to power generation at the point of consumption. Generating power on-site rather than centrally, eliminates the cost, complexity, interdependencies and inefficiencies associated with transmission and distribution.

Hybrid power generation systems appear to be a promising source of distributed power generation because of the high fuel to electricity conversion efficiency and low negative effects on the environment. Hybrid power generation systems are a combination of conventional heat engines and fuel cells. High temperature fuel cells are found to be most suitable for hybrid operation. The high operating temperature of these fuel cell systems allows integration with a gas turbine engine at a temperature which is mutually beneficial. Depending on the design of integrated hybrid system, waste heat from the fuel cell could be converted in the gas turbine engine to electricity or waste heat from the gas turbine could be put to good use preheating reactants for the fuel cell or for providing energy for fuel processing.

Fuel cells are electrochemical devices capable of converting chemical energy of a fuel directly to usable energy – electricity and heat – without combustion. Power generation devices like steam turbines, gas turbines, reciprocating engines convert the chemical energy of fuel to thermal energy, then to mechanical energy and then to electricity. The performance of a fuel cell is not restricted by Carnot Law constraints that

limit heat engine efficiencies. The electrical conversion efficiency of most fuel cells ranges from 40 to 60 percent [1].

Fuel cells are classified into various categories such as Proton Exchange Membrane Fuel Cell (PEM), Direct Methanol Fuel Cell (DMFC), Alkaline Fuel Cell (AFC), Phosphoric Acid Fuel Cell (PAFC), Molten Carbonate Fuel Cell (MCFC) and Solid Oxide Fuel Cell (SOFC) depending upon the type of electrolyte used, nature and type of fuel used, method of fuel processing and temperature of operation. SOFC has various advantages over other types of fuel cells considering application in hybrid systems. A wide range of fuels can be used in SOFC system since the higher operating temperature allows for internal reforming. Considering the current developed infrastructure for supply of hydrocarbon fuels, SOFC hybrid system is well suitable for distributed power generation. The high operating temperature supplies high quality waste heat for cogeneration. SOFC system is more tolerant to presence of impurities in reactant gases. A hybrid SOFC-GT system can achieve up to 75% fuel to electric efficiency [2].

1.1.1 Solid Oxide Fuel Cell – Gas Turbine Hybrid System

A fuel cell fundamentally consists of an electrolyte (an ion containing solution, liquid or solid) in contact with two electrodes. One electrode is the Anode (positive electrode), where oxidation of fuel occurs. Another electrode is the Cathode (negative electrode) where reduction of oxygen occurs. A typical fuel cell requires gaseous fuel and oxidant flows. Hydrogen is the preferred fuel because of its high reactivity, which minimizes the need for expensive catalysts. Another advantage of using hydrogen is that, the electro-oxidation of hydrogen leads only to water emission.

Solid oxide fuel cells have operating temperatures in the range of 800^0C to 1100^0C. The electrolyte used is Yttria Stabilized Zirconia (YSZ). Anode is a cermet of metallic nickel and YSZ skeleton. Cathode is Strontium doped Lanthanum Magnetite. A

fuel, generally hydrogen (H_2) is supplied to the anode side of fuel cell. Here, hydrogen reacts with oxide ions from electrolyte thereby releasing electrons to the external circuit.

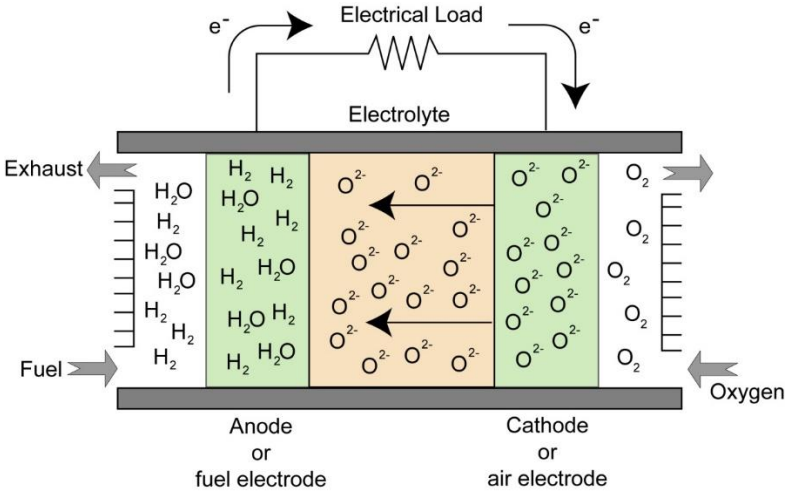

Figure 1-1 Working of Fuel Cell

The anode reaction is as follows.

$$H_2 + O^{2-} \rightarrow H_2O + 2e^-$$

On the cathode side, an oxidant, generally air or oxygen is supplied. Here, it accepts electrons from the external circuit and supplies oxide ions (O^{2-}) to the electrolyte. The cathode reaction is given as follows.

$$\frac{1}{2} O_2 + 2e^- \rightarrow O^{2-}$$

Overall reaction is given as follows.

$$H_2 + \frac{1}{2} O_2 \rightarrow H_2O$$

The ions created by electrochemical reaction flow between anode and cathode through the electrolyte. Electrons produced at anode flow through an external load to cathode completing an electric circuit. Solid Oxide fuel cells have higher overall fuel to electricity efficiency than lower temperature fuel cells operated on available hydrocarbon fuels.

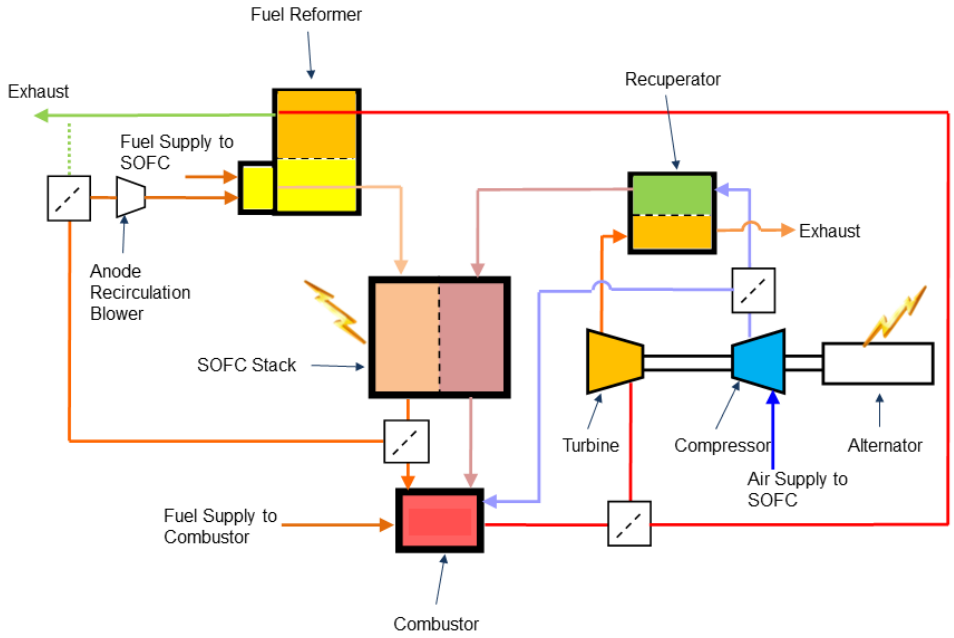

Figure 1-2 Solid Oxide Fuel Cell - Gas Turbine Hybrid System

The hybrid system combines SOFC with low-pressure-ratio gas turbine, air compressor, combustor, fuel compressor, fuel processing unit and air preheater. The SOFC and gas turbine operate in cogeneration by using rejected thermal energy and residual fuel from the fuel cell to operate the gas turbine. The gas turbine combustor is an external one in which residual fuel from anode side is mixed with high temperature air exhaust from cathode side and burned, in order to raise the gas turbine inlet temperature.

In the hybrid cycle shown, air is compressed by air compressor up to a value, little higher than SOFC operating pressure. The air is then preheated in a recuperator which is a counter-flow plate-fin heat exchanger using energy from the turbine exhaust. As a result waste heat energy from the turbine exhaust is recovered in pre-heating the air

supplied to SOFC cathode side. Similarly, fuel (methane) is compressed by a fuel compressor and supplied to the fuel processing unit. Here the fuel mixes with anode recirculation exhaust. The energy required for fuel processing and raising temperature of the mixture to required operating temperature, is absorbed from a fraction of the hot gases exiting combustor, supplied to fuel processing unit. The most effective design for fuel reformer is found to be a counter-flow plate-fin type heat exchanger with catalyst coated fins [3]. Any non-reformed fuel is then internally reformed within the anode channel of SOFC.

The ionic and electronic currents which are generated then complete a circuit from which DC power is generated. This DC power is converted into AC power using an inverter. The energy released in fuel cell from chemical interactions is used for internal reforming and to maintain temperature of fuel cell stack. The exhaust from anode side is divided into two streams. One stream is supplied to anode recirculation blower, to again enter the SOFC stack. Another stream is supplied to the combustor. The high temperature exhaust air from cathode side is supplied to combustor where it is used to burn the residual fuel. A specific amount of extra fuel and a fraction of air from compressor outlet is also supplied to the combustor to maintain optimum air to fuel ratio in combustor. The high temperature and high pressure gases from combustor are then supplied to the turbine. The gases expand in turbine and power generated is used to drive the compressor and also run an alternator to produce electricity. The exhaust from turbine is still at very high temperature. This energy content of turbine exhaust is used to preheat the air supplied to cathode of SOFC. This heat exchange is brought about in the recuperator. The recuperator and the fuel reformer are ‘waste heat recovery systems’ in the hybrid cycle which help in reducing operating cost of the cycle. The design of

recuperator and fuel reformer are critical for economical of the system. The recuperator considered for this system is of plate-fin type with counter flow configuration.

1.2 Plate Fin Heat Exchangers

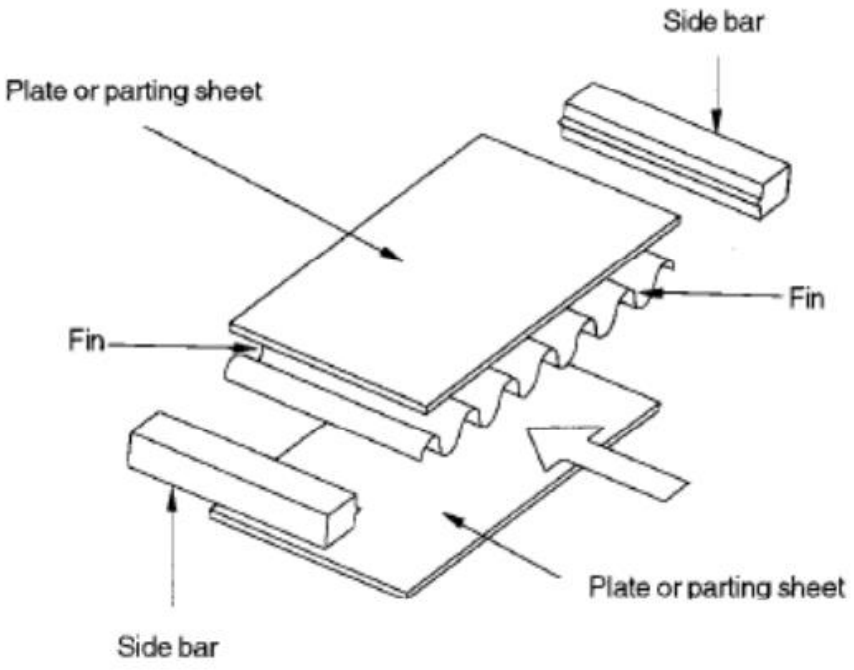

Figure 1-3 Plate Fin Heat Exchanger Split View

The plate-fin type of heat exchangers have gained wide acceptance in industry because of their superior performance and cost-effectiveness as compared to various other compact heat exchangers. The plate fin heat exchanger is essentially a stack of alternating layers of flat plates and corrugated fins, bonded together to form a monolithic block for distinct passages of fluid streams. Primary mode for heat transfer between fluid is the separating plate and secondary mode is the fins connected to primary surface. The fins aid heat transfer process and also provide rigidity to the structure against internal pressure. Side bars also bonded to the plates, prevent fluid streams from spilling over or mixing among each other.

1.2.1 Advantages and Disadvantages

Plate-fin heat exchangers offer several advantages as compared to other types of heat exchangers. They are listed as follows:

1) Compactness: Plate-fin heat exchangers generally provide large heat transfer area per unit volume, typically $1000\ m^2/m^3$. Small passage size produces a high overall heat transfer coefficient.

2) Effectiveness: Values of thermal effectiveness of around 95% can be obtained.

3) Temperature Control: The plate-fin heat exchanger can operate with small temperature differences. A close temperature approach (temperature approach as low as 3K) is obtained for a heat exchanger, exchanging heat with single phase fluid streams. This is an advantage when high temperatures need to be avoided. Local overheating and possibility of stagnant zones can also be reduced by the form of flow passages.

4) Flexibility: Changes can be made to heat exchanger performance by utilizing a wide range of fluids and conditions that can be modified to adapt to various design specifications. Multi stream operation is also possible.

5) Counter Flow Configuration: A perfect counter flow configuration, unlike the shell and tube heat exchanger where the shell flow is usually a mixture of cross and counter flow, is possible in a plate-fin heat exchanger.

The main disadvantages of a plate-fin heat exchanger are as follows:

1) The rectangular geometry used puts a limit on operating range of pressures and temperatures.

2) There is difficulty encountered in cleaning of passages, which limits its application to clean and relatively non-corrosive fluids.

3) There is difficulty of repair in case of failure or leakage between passages.

4) Fluid experiences relatively high pressure drop due to narrow and constricted passages.

1.2.2 Materials and Manufacturing Process

The materials of construction are generally alloys of aluminium or stainless steel, the choice of which is dependent on process temperature and operating pressures. Aluminium alloys are particularly suitable for low temperature applications because of their excellent thermal properties, low weight, excellent ductility and increased strength at high temperatures. The basic principles of plate-fin heat exchanger manufacturing are same for all sizes and all materials. The heat exchanger is assembled from a series of flat sheets and corrugated fins in a sandwich construction. Separating plates provide the primary heat transfer surface. Separating plates are positioned alternatively within layers of fins in the stack to form containment between individual layers. The corrugations, side bars, parting sheets and cap-sheets are held together in a jig under a predefined load, and placed in a brazing furnace to form the plate fin heat exchanger block. After this, the header tanks and nozzles are welded to the block, taking care that brazed joints remain intact during welding process. The most common methods used for brazing are salt bath brazing and vacuum brazing.

1.2.3 Applications

Plate-fin heat exchangers are used in variety of applications, the most notable among them are cryogenic liquefaction and separation of air, processing and liquefaction of natural gas, production of petrochemicals and large refrigeration systems [4]. Heat exchangers used for cryogenic air separation and LPG fractionation, are the largest and most complex units of plate-fin type. A single unit of such type can be of several meters in length and up to $1.2m \times 1.2m$ in cross-section. Brazed aluminium plate-fin heat exchangers find wide applications in aerospace industry due to their low weight and high

compactness. In the aircraft they are used in the environment control system, for cooling of avionics and hydraulic oil, and for fuel heating. Other major applications of plate-fin heat exchangers include automobile and HVAC systems. A modern automobile contains nearly half a dozen heat exchangers, which is expected to double with the introduction of fuel cell technology. Making the heat exchangers more compact is of high importance for applications in distributed power generation, automobile and air conditioning industries.

1.2.4 Flow Arrangement

A plate-fin heat exchanger has two or more streams which may flow in directions parallel or perpendicular to one another. When flow directions are parallel, streams may flow in the same or in opposite sense. Hence the three primary flow arrangements can be said to be parallel-flow, counter-flow and cross-flow. Thermodynamically the counter-flow configuration provides highest energy absorption or rejection, while the parallel-flow arrangement provides lowest. The cross-flow arrangement delivers a performance intermediate to those of counter-flow and parallel-flow. Cross-flow configuration offers superior heat transfer properties and easier mechanical layout. The heat exchanger under study has a counter-flow arrangement.

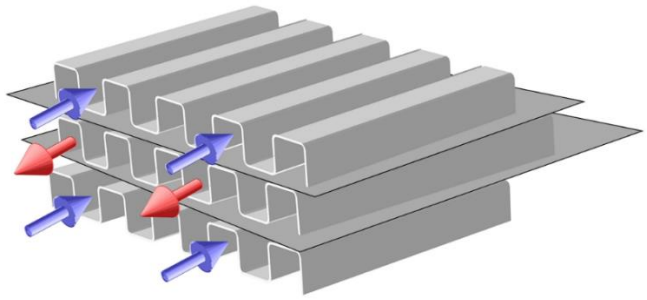

Figure 1-4 Counter-flow Plate Fin Heat Exchanger

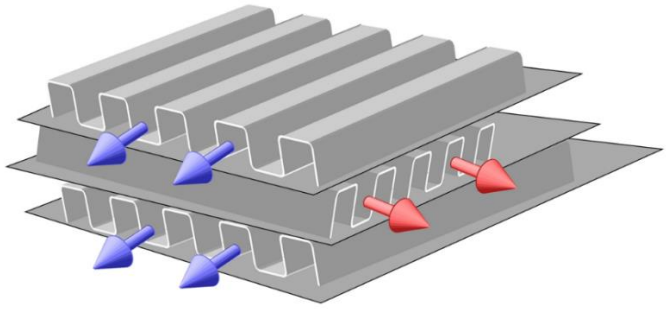

Figure 1-5 Cross-flow Plate Fin Heat Exchanger

In a counter-flow configurations, the fluids flow parallel to each other, but in opposite directions. The counter-flow arrangement is thermodynamically superior to any other configuration. It is the most effective flow arrangement producing higher temperature change in each fluid compared to any other two-fluid arrangements for a given overall thermal conductance, fluid flow rates and fluid inlet temperatures. Cryogenic refrigeration and liquefaction equipment use this geometry almost exclusively. These type of heat exchangers demand proper design due to complex geometry of headers.

1.3 Extended Heat Transfer Surfaces

The plate-fin heat exchangers are mainly employed for liquid-to-gas and gas-to-gas applications. Due to low heat transfer coefficients in gas flows, extended surfaces are commonly employed in plate-fin heat exchangers. By using specially configured extended surfaces, heat transfer coefficients can also be enhanced. While such special surface geometries provide much higher heat transfer coefficients than plain extended surfaces, the pressure drop penalties are also high, though they may not be severe enough to negate the thermal benefits. A variety of extended surface like the plain rectangular, plain

trapezoidal, wavy, offset strip fin and more are used. The plain corrugated type geometry is considered in the current study.

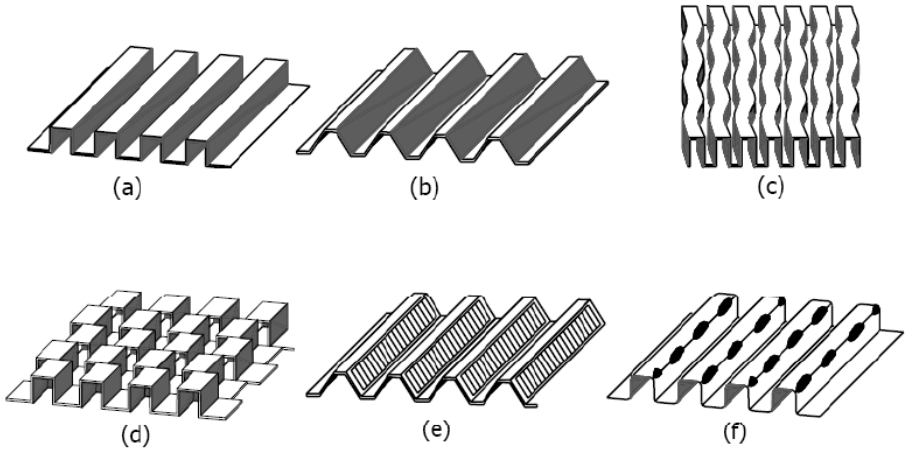

Figure 1-6 Various Fin Geometries for Plate Fin Heat Exchangers (a) Plain Rectangular (b) Plain Trapezoidal (c) Wavy (d) Serrated or Offset Strip Fin (e) Louvered (f) Perforated

In order to improve the heat transfer coefficients, the surface features need to be provided. These features are divided into two categories. First, in which the surface remains continuous and the second in which it is cut. In a continuous type fin the corrugations cause the gas to make sudden direction changes so that locally the velocity and temperature gradients are increased. This results in local enhancement of heat transfer coefficient. But an undesirable consequence of such enhancement in heat transfer coefficient is an increase in the friction factor and pressure drop, whereas in a discontinuous type of fin geometry, boundary layers are interrupted.

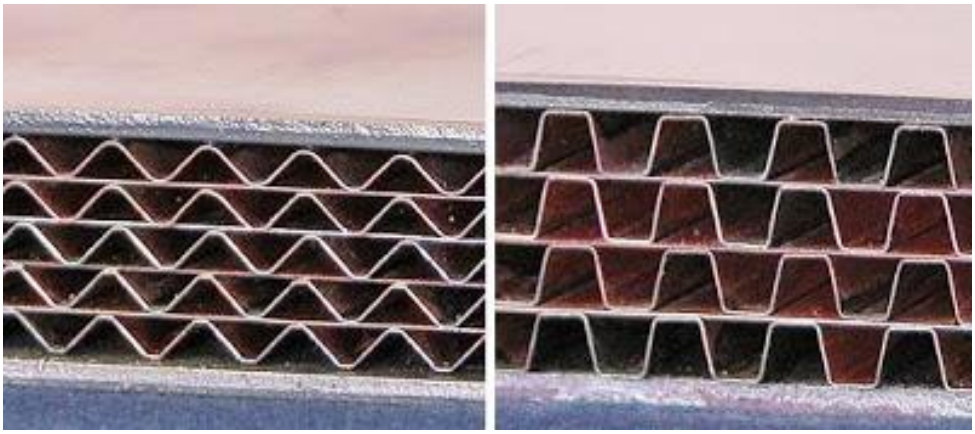

Figure 1-7 Corrugated Fins

Adjacent to the leading edge of the fin, both heat transfer coefficient and friction factor are high due to generation of fresh boundary layers. But in addition to this friction drag, form drag is also generated due to the finite thickness of the fin. Although friction drag is associated with high heat transfer coefficient, form drag has no counterpart and represents one form of wasted energy. The form drag can be substantial depending on the quality of the cutting edge. However, machined-formed fins are generally free from this problem.

1.4 Thesis Objective

The objective of this thesis is to develop a computational solver for simulating steady state performance of a plate-fin heat exchanger with counter-flow arrangement. The motive for solver development is to integrate the numerical model with a cycle simulating 'Solid Oxide Fuel Cell - Gas turbine Hybrid System'. This model can be integrated with any other complex system solver and can also be used as a stand-alone simulator for a plate-fin heat exchanger. The better the approximation of thermal-fluid behavior of a system, the more effortless and transparent is process of designing experimental setup or product. The numerical model can also simulate co-flow arrangement with some changes in formulation.

1.5 Organization of Thesis

The thesis has been arranged in six chapters. Chapter 1 explains the application of recuperator for waste heat recovery in a hybrid power generation system. It also gives an overview about plate fin heat exchangers, their advantages and characteristics. Chapter 2 gives a brief review of relevant literature. The beginning part of Chapter 3 gives an introduction to finite volume method and the Advection-Diffusion equation. The following part of Chapter 3 explains recuperator geometry and energy interaction model in detail, which is followed by a comprehensive explanation of mathematical formulation of the solver and procedure of operation. Chapter 4 deals with validation of the computational model by comparing simulation results with heat transfer textbooks and published literature. The validation part is followed by a demonstration of, how the solver can be used as a stand-alone system for heat exchanger simulation. Chapter 5 contains the conclusion and Chapter 6 gives future scope for development.

Chapter 2

LITERATURE REVIEW

The purpose of a recuperative heat exchanger is to facilitate effective exchange of thermal energy between two fluid streams flowing continuously on opposite sides of a solid partition. The plate fin heat exchanger has proven to be an excellent engineering solution, satisfying the diverse requirements of high efficiency, compactness and reliability in many applications. During process of heat exchange, the streams experience viscous resistance, which gives rise to pressure drop. The quantity of heat transfer and the magnitude of the pressure drop are the performance parameters chosen to describe a heat exchanger. Due to their extensive practical applications, heat exchangers have attracted attention of a large number of researchers over the years. Investigations involving applied as well as fundamental research, experimental as well as theoretical studies have been reported in literature. While some of the research outcome falls in proprietary domain, a substantial part of it is available in open literature.

Fundamental relations describing various types of heat transfer phenomena and heat exchanger design techniques have been discussed in text books [5-11]. The book “Compact Heat Exchangers” by Kays and London [5] provides an excellent introduction to the analysis of plate fin heat exchangers, and contains a valuable database on the heat transfer and flow friction characteristics of several fin geometries. The work of Shah [10-11] provides one of the most comprehensive information on the subject, particularly on compact plate-fin heat exchangers. Shah [23], while discussing the classification of heat exchangers, defines ‘compact heat exchanger’ as one having an area density greater than $700\ m^2/m^3$. Such compactness is achieved by providing a high density of fins in the flow passages.

Journals on thermal engineering and heat transfer devote a sizable portion of their content to research findings on heat exchangers [12-15]. Two major journals: Heat Transfer Engineering [16] and International Journal of Heat Exchangers [17] are almost exclusively dedicated to the subject of heat exchangers.

One of the earliest and most comprehensive experimental works on compact heat exchangers was carried out by Kays and London at Stanford University in late 1940. Their report [18] published in 1948 gives the complete methodology and details of the experimental set up. Several researchers used the same experimental technique for experimental determination of non-dimensional heat transfer coefficient and friction factor. Later on, several empirical correlations were generated from the experimental data of Kays and London and other experimental works.

The performance of heat exchangers with no axial conduction, property variations or heat leakage can be determined using the effectiveness-NTU relations that are reported in many textbooks. The large absolute temperature changes within the heat exchanger produce correspondingly large variations in properties of the fluids and metal that can also affect performance. There have been several papers that have considered some of these effects. For example, Kays and London [5] present graphical results for the performance deterioration of a balanced and near balanced counter-flow heat exchanger due to axial conduction. Kroeger [19] presents a comprehensive, analytical study of the effect of axial conduction on a counter-flow heat exchanger.

Narayanan and Venkatarathnam [20] present a closed form equation for unbalanced counter-flow heat exchangers with axial conduction at very high NTU. Chowdhury and Sarangi [21] present an analytical solution for the case where a heat leak from ambient, assumed to be linearly proportional to temperature difference, is forced into the cold fluid. Nellis [22] derives the governing equations for heat exchanger in a

finite difference form. The numerical results are validated by considering global energy conservation and through comparison with the analytical studies mentioned above in the appropriate limits.

Chapter 3

MATHEMATICAL MODELING

3.1 Finite Volume Method

Finite volume method is a discretization method which is well suited for numerical simulation of various types of conservation laws. It has been extensively used in various engineering fields such as fluid mechanics, heat and mass transfer and petroleum engineering. Finite volume method may be used on arbitrary geometries, using structured or unstructured meshes, and it leads to robust schemes. An additional feature is local conservation of numerical fluxes, that is the numerical flux is conserved from one discretization cell to its neighbor. This feature makes the finite volume method quite attractive when modelling problems for which flux is of importance, such as fluid mechanics, heat and mass transfer or semi-conductor device simulation. The finite volume method is locally conservative because it is based on a balance approach. A local balance is written on each discretization cell, which is often called a control volume. Using divergence formula, an integral formulation of fluxes over boundary of the control volume is obtained. The fluxes on the boundary are discretized with respect to discrete unknowns.

Basic Methodology:

1) Divide the domain into control volumes

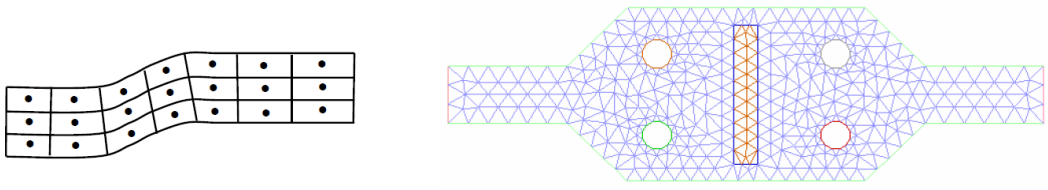

Figure 3-1 Finite Volume Grids

2) Integrate differential equation over the control volume and apply divergence theorem.

3) In order to evaluate derivative terms, the values at control volume faces are needed. We have to make an assumption about how the value varies.

4) Result is a set of linear algebraic equations, one for each control volume.

5) Solve iteratively or simultaneously.

In finite volume method, the domain under consideration is divided into a finite number of control volumes (cells) by a grid. Grid defines boundaries of control volume while the computational node lies at the center of control volume. The advantage of finite volume method is that, the integral conservation is satisfied exactly over the control volume.

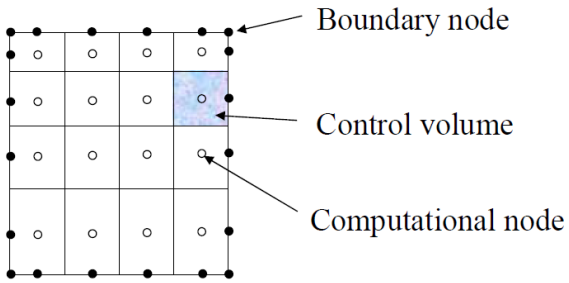

Figure 3-2 Finite Volume Cell Arrangement Overview

The net flux through control volume boundary is sum of integrals over the four control volume faces (six faces for 3D). The control volumes do not overlap. The value of integrand is not available at control volume faces and is determined by interpolation.

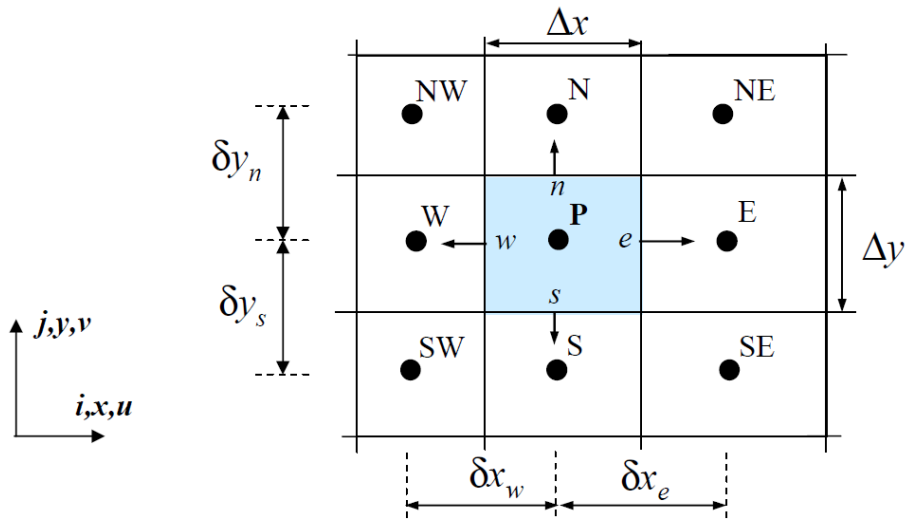

Figure 3-3 Finite Volume Cell Arrangement for 2-D Mesh

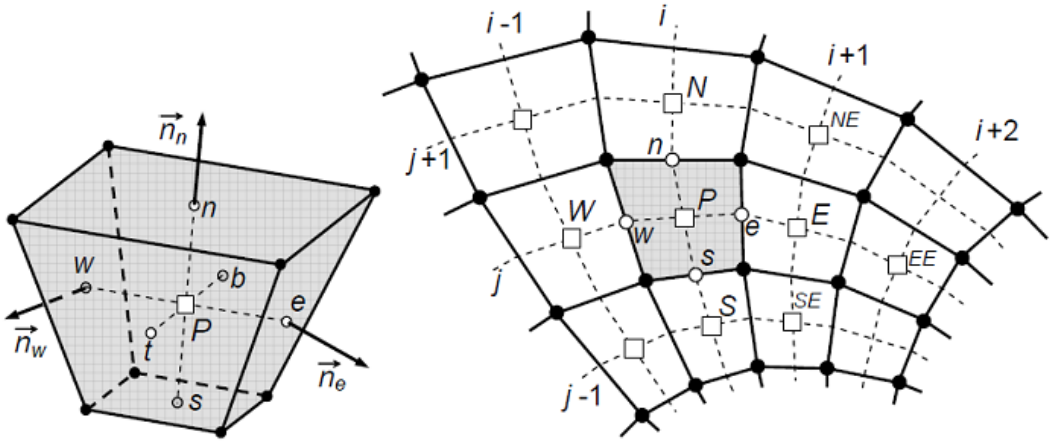

Figure 3-4 Finite Volume Cell Arrangement for 3-D Mesh

The finite volume method is quite different from the finite difference method or the finite element method. Roughly speaking the principle of finite difference method is, given a number of discretization points which may be defined by a mesh, to assign one discrete unknown per discretization point, and to write one equation per discretization

point. At each discretization point, derivatives of the unknown are replaced by finite differences by the use of Taylor expansions. Finite difference method becomes difficult to use when coefficients involved in the equation are discontinuous. In the case of finite volume method, discontinuities of coefficients will not be any problem if the mesh is chosen such that discontinuities of coefficients occur on the boundaries of control volumes. Indeed in finite volume formulation, finite difference approach can be used for approximation of fluxes on the boundary of control volumes. From the industrial point of view, the finite volume method is known as a robust and computationally less expensive method for the discretization of conservation laws. Robust particularly stands for, a scheme which behaves well even for particularly difficult equations, such as nonlinear systems of hyperbolic equations and which can easily be extended to more realistic and physical contexts than the classical academic problems.

3.2 The Advection-Diffusion Equation

In nature, transport occurs in fluids through the combination of advection and diffusion. Diffusion phenomenon can be considered to be the transport of mass, momentum or energy by virtue of concentration difference. Advection physics can be considered to be the transport of mass, momentum or energy because of bulk motion.

$$\frac{\partial(\rho\Phi)}{\partial t} + \nabla\cdot(\rho V\Phi) = \nabla\cdot(\Gamma\nabla\Phi) + S \tag{1}$$

The four terms are ‘Unsteady term’, ‘Convection term’, ‘Diffusion term’ and ‘Source term’.

In general, $\Phi = \Phi(x, y, z, t)$

Γ is the diffusion coefficient corresponding to the particular property Φ.

As Φ takes different values, we get conservation equations for different quantities.

$\Phi = 1$: Conservation of Mass

$\Phi = u$: Conservation of Momentum

$\Phi = h$: Conservation of Energy

The differential equation when integrated over the control volume give following form.

$$\int_{CV}\left(\int_{t}^{t+\Delta t}\frac{\partial}{\partial t}(\rho\Phi)dt\right)dV + \int_{t}^{t+\Delta t}\left(\int_{A} n\,(\rho V\Phi)\,dA\right)dt$$

$$= \int_{t}^{t+\Delta t}\left(\int_{A} n\,(\Gamma\nabla\Phi)\,dA\right)dt + \int_{t}^{t+\Delta t}\left(\int_{CV} S\;dV\right)dt$$

For simplicity, we will consider a steady and 1-D case, with no source term.

$$\frac{d}{dx}(\rho u\Phi) = \frac{d}{dx}\left(\Gamma\frac{d\Phi}{dx}\right) \tag{2}$$

The flow field should also satisfy the continuity equation.

$$\frac{d}{dx}(\rho u) = 0 \;or\; \rho u = constant$$

Consider the following finite volume.

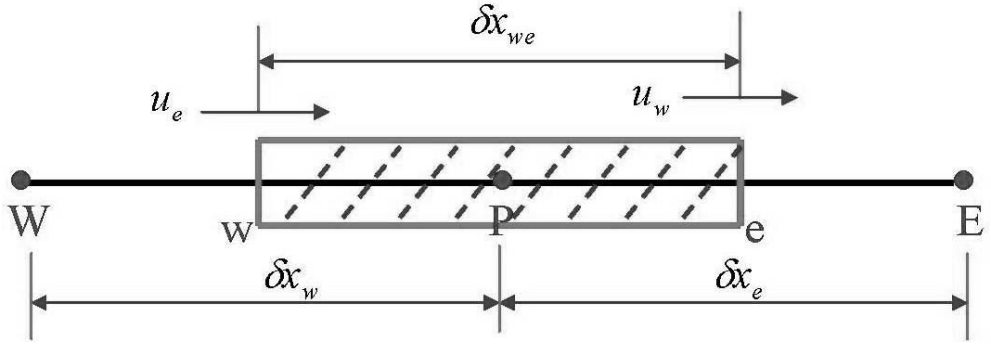

Figure 3-5 1-D Finite Volume

Integration of transport equation (2) over the control volume gives,

$$(\rho uA\Phi)_e - (\rho uA\Phi)_w = \left(\Gamma A\frac{\partial\Phi}{\partial x}\right)_e - \left(\Gamma A\frac{\partial\Phi}{\partial x}\right)_w \tag{3}$$

The derivatives for diffusion term are calculated assuming piecewise linear profile of Φ.

$$\left(\Gamma A \frac{\partial \Phi}{\partial x}\right)_e = \Gamma_e A_e \left(\frac{\Phi_E - \Phi_P}{\delta x_e}\right)$$

$$\left(\Gamma A \frac{\partial \Phi}{\partial x}\right)_w = \Gamma_w A_w \left(\frac{\Phi_P - \Phi_W}{\delta x_w}\right)$$

Assuming, $A_e = A_w$, equation (3) becomes,

$$F_e \Phi_e - F_w \Phi_w = D_e (\Phi_E - \Phi_P) - D_w (\Phi_P - \Phi_W)$$

Where, $F = \rho u$ and $D = \frac{\Gamma}{\delta x}$ are, convection and diffusion factors respectively.

$$F_w = (\rho u)_w, F_e = (\rho u)_e$$

$$D_w = \frac{\Gamma_w}{\delta x_w}, D_e = \frac{\Gamma_e}{\delta x_e}$$

From the continuity equation, $F_w = F_e$

There are various schemes which are used to approximate value of Φ on the faces.

Some of them are explained as follows.

1) First Order Upwind Scheme:

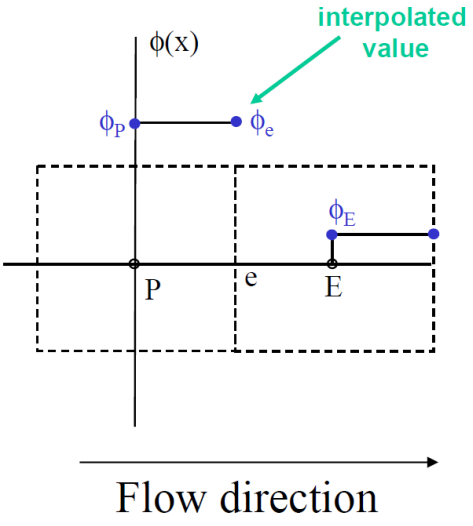

Figure 3-6 First Order Upwind Scheme

This is the simplest numerical scheme. We assume that value of Φ at the face is same as the cell centered value in cell upstream of the face. The main advantages are that it is easy to implement and it results in very stable calculations, but it also very diffusive. Gradients in the flow field tend to be smeared out. This is often the best scheme to start calculations with.

2) Central Differencing Scheme:

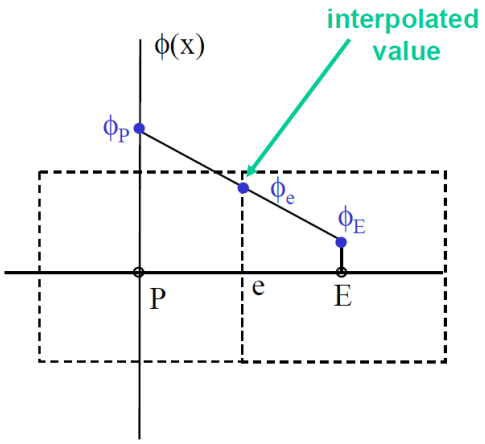

Figure 3-7 Central Differencing Scheme

In this scheme we determine value of Φ at the face by linear interpolation between cell centered values. This is more accurate than first order upwind scheme, but it leads to oscillations in the solution or divergence if local Peclet number is larger than 2. Peclet number is the ratio of convective to diffusive factors.

$$Pe = \frac{F}{D}$$

It is common to, switch to first order upwind in cells where $Pe > 2$. Such an approach is called a hybrid scheme.

3) Power Law Scheme:

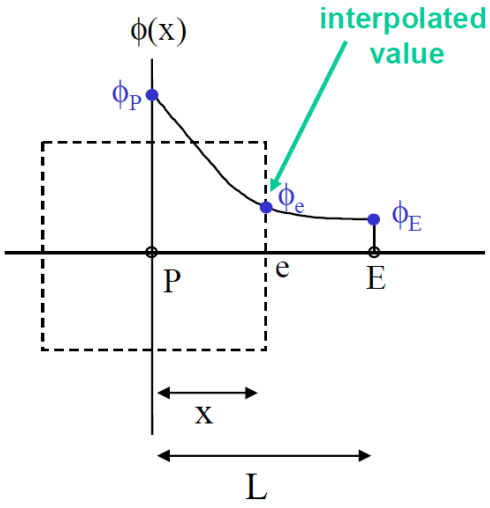

Figure 3-8 Power Law Scheme

This scheme is based on the analytical solution of one-dimensional advection-diffusion equation. The face value is determined from an exponential profile fitted through cell values. The exponential profile is approximated using following power law equation.

$$\Phi_e = \Phi_P - \frac{(1 - 0.1\,Pe)^5}{Pe}(\Phi_E - \Phi_P)$$

For values of Pe greater than 10, diffusion is ignored and first order upwind scheme is used.

4) Second-order Upwind Scheme:

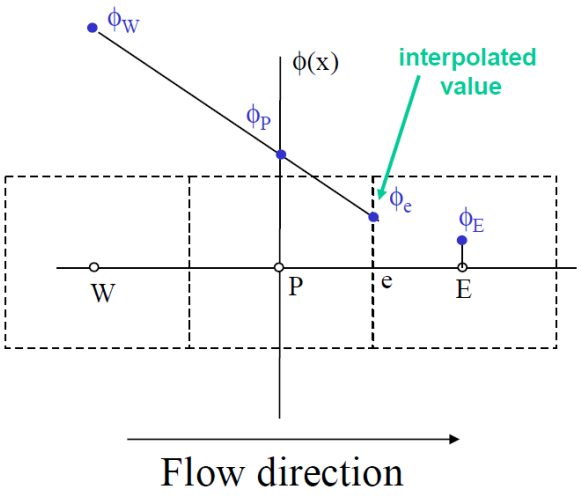

Figure 3-9 Second Order Upwind Scheme

Value of Φ is determined using cell values in two cells upstream of the face. This is more accurate than first order upwind scheme, but in regions with strong gradients, it can result in face values that are outside the range of cell values. It is then necessary to apply limiters to the predicted face values. There are many different ways to implement this, but second order scheme with limiters is one of the most popular numerical schemes because of its combination of accuracy and stability.

5) QUICK Scheme:

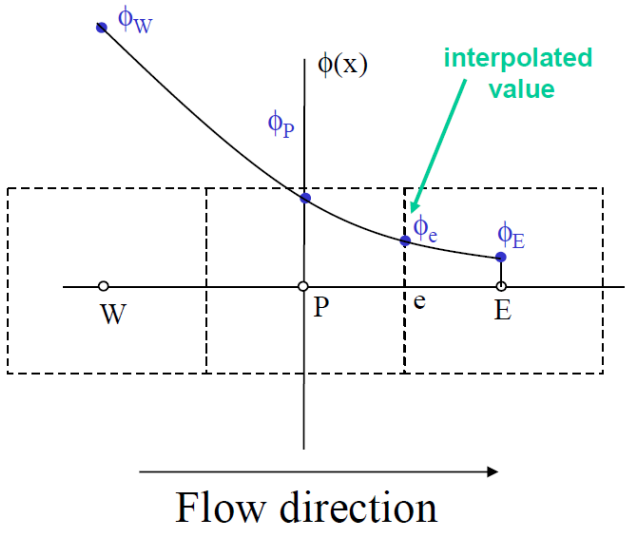

Figure 3-10 QUICK Scheme

QUICK stands for Quadratic Upwind Interpolation for Convective Kinetics. A quadratic curve is fitted through two upstream nodes and one downstream node. This is a very accurate scheme, but in regions with strong gradients, overshoots and undershoots can occur. This can lead to stability problems in the calculation.

Finally we get an equation of the form,

$$a_P \Phi_P = a_W \Phi_W + a_E \Phi_E + b$$

We solve iteratively for Φ_P.

3.3 Model Overview

The air pre-heater is used to heat air supplied to cathode side of the fuel cell stack. Air coming out from the turbine outlet is at a considerably high temperature. The energy content of this air stream can be transferred to air supplied to the stack through a heat exchanger, thereby reducing the net energy input to the system.

The heat exchanger used is a plate-fin type counter-flow heat exchanger. The modeling of heat exchanger is done using finite volume discretization scheme. The fluid

flow in hot and cold fluid channels is simulated using advection-diffusion equation. Diffusion can be considered to be the net movement of energy from high concentration to low concentration. Advection is the transport of energy by means of bulk motion. Solver simulates the two physics to predict properties of hot and cold fluids at outlets. Heat transfer in the middle plate and fins is modelled using diffusion equation with source term.

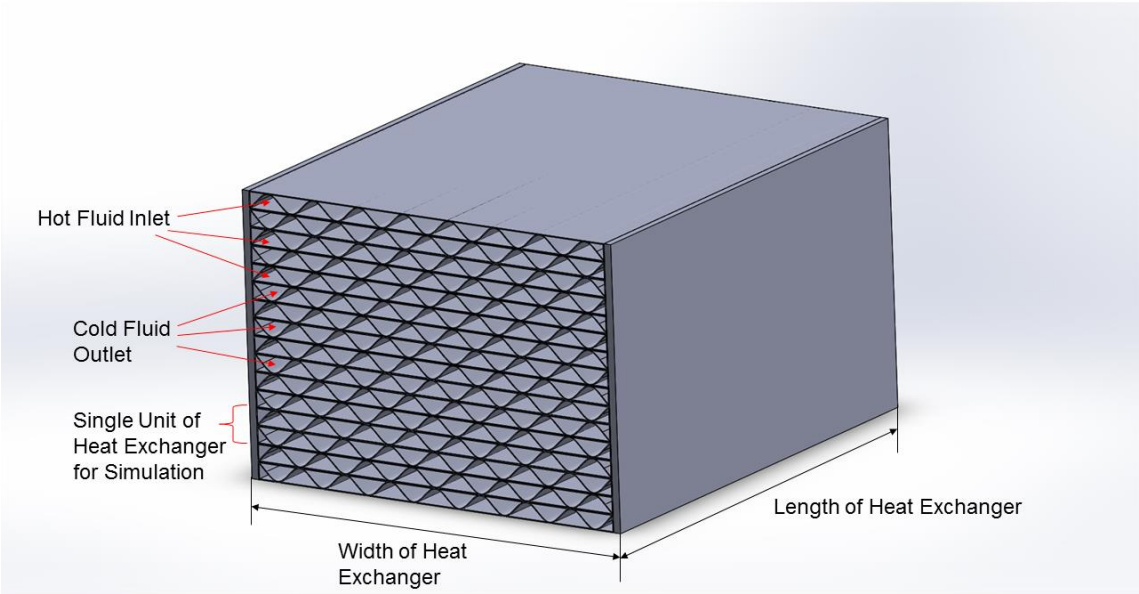

Figure 3-11 Heat Exchanger Core Schematic

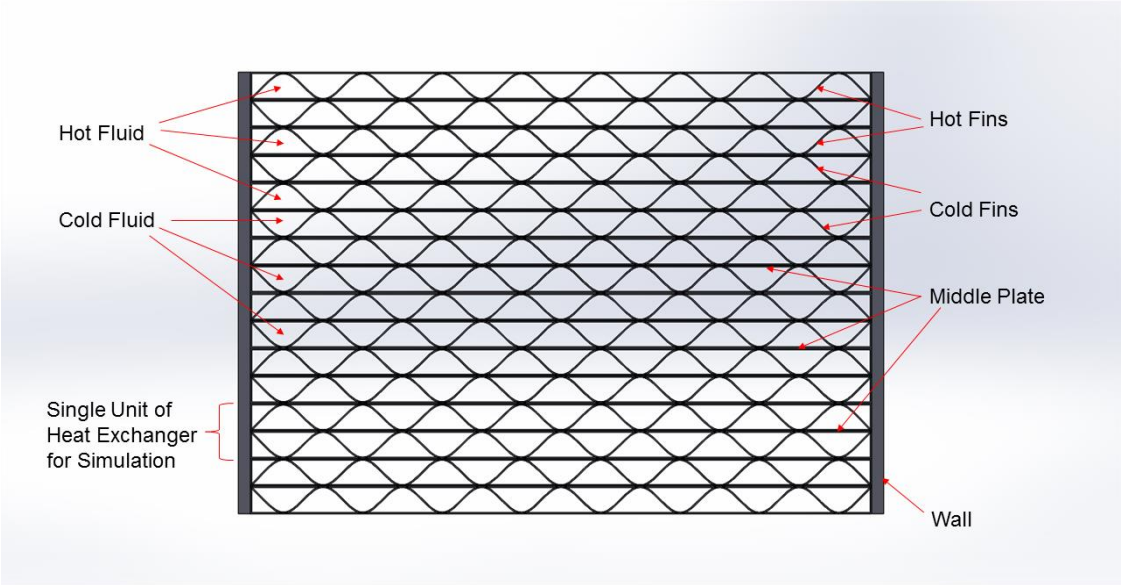

Figure 3-12 Heat Exchanger Core Channel Cross-section

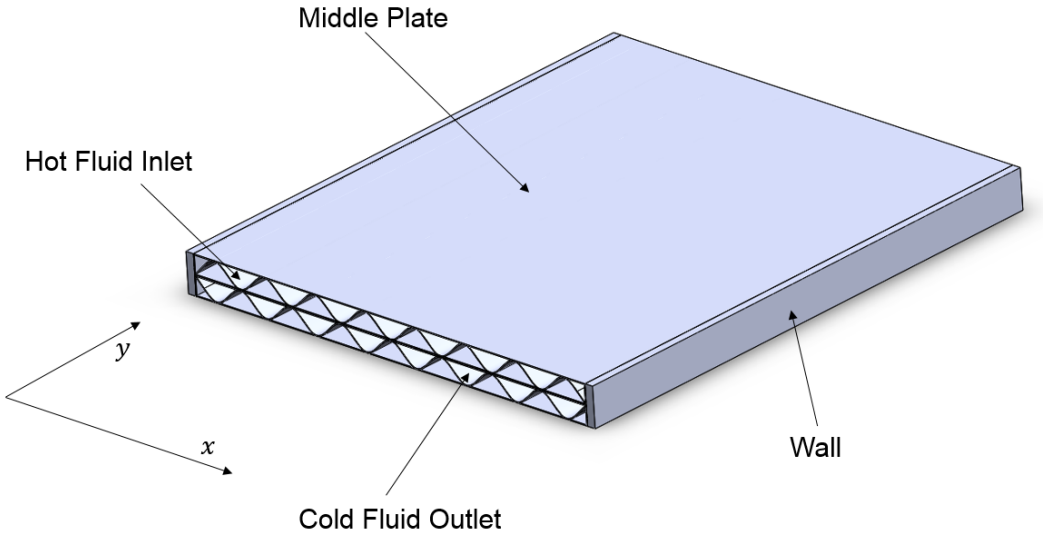

Figure 3-13 Unit Module Chosen for Simulation

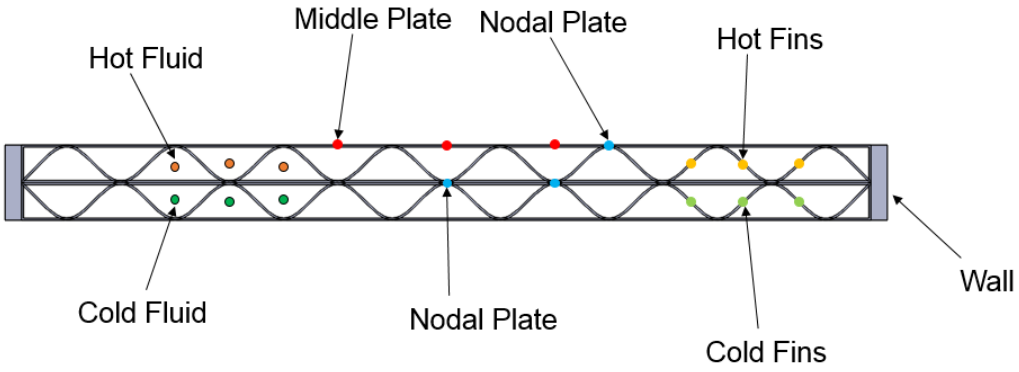

Figure 3-14 Heat Exchanger Unit Module Nodal Configuration

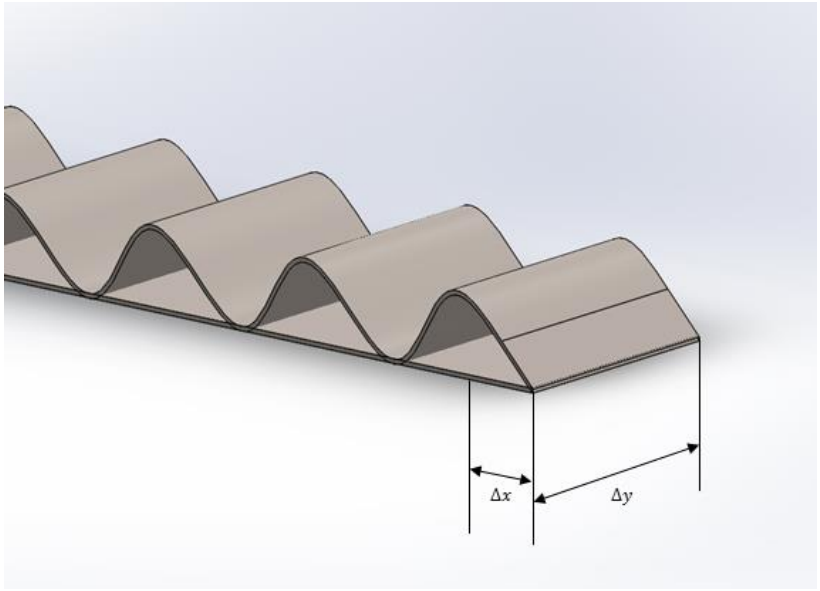

Figure 3-15 Fin Overview

The heat transfer from hot fluid to cold fluid is modeled in two ways. First or primary mode is, convective heat transfer from hot fluid to middle plate and subsequent convective heat transfer from middle plate to cold fluid. The secondary mode is in the given order, convective heat transfer from hot fluid to hot fins, conductive heat transfer

from hot fins to middle plate, conductive heat transfer from middle plate to cold fins and convective heat transfer from cold fins to cold fluid.

The middle plate is divided into two parts for simplicity and efficiently modelling heat transfer. The ‘Nodal Plate’ is a part of middle plate and is used to consider conductive heat transfer from fins to parting plate. The fins are connected to nodal plate finite volumes and interact with the later. The configuration is considered to be an infinite stacking for current modeling purposes. Therefore only one unit of heat exchanger core is simulated. The model can be extended to multiple units subsequently. Primary mode of heat transfer is shown in the following figure.

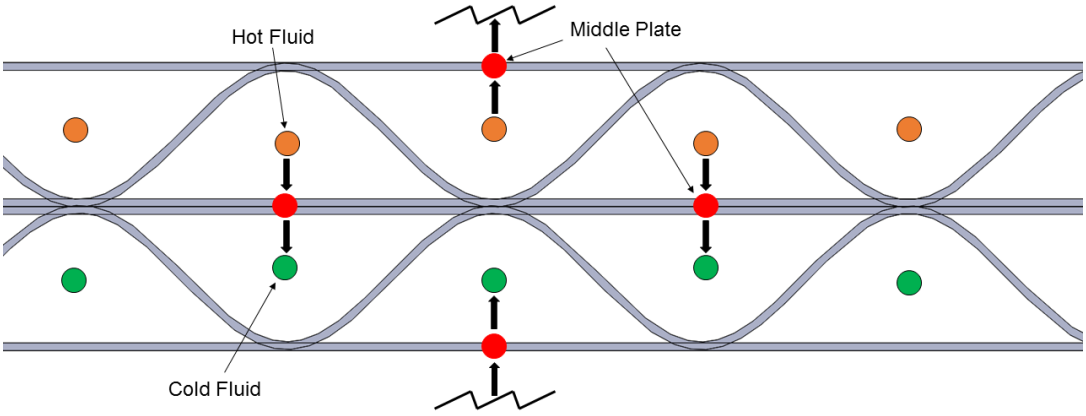

Figure 3-16 Primary Heat Transfer Mode

The secondary mode of heat transfer is shown in the following figure.

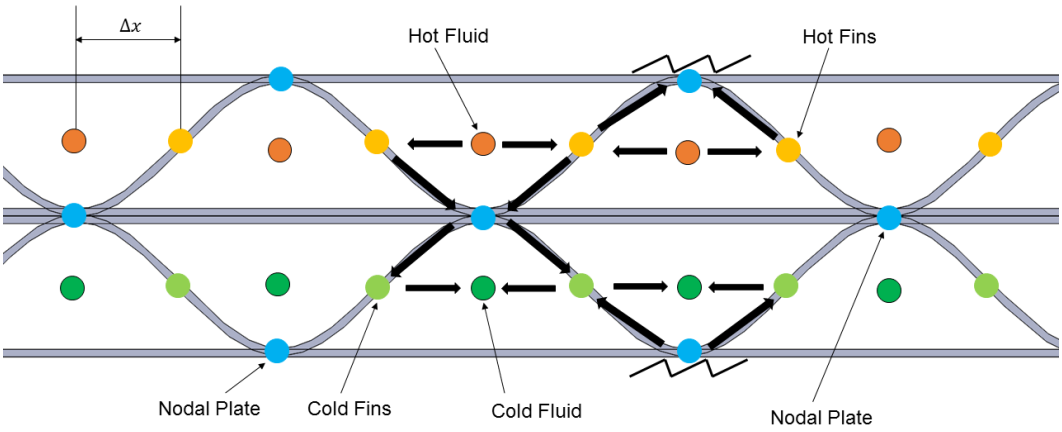

Figure 3-17 Secondary Heat Transfer Mode

The number of finite volumes of fluid channels, plates and fins are essentially equal along the flow direction.

3.4 Methodology

Programming language used to develop the solver is C++. The IDE used is Visual Studio 2015. Post-processing is performed using MATLAB R2013A. The model solves iteratively for mass flow rates and temperatures across the field. Following flowchart describes fundamental methodology of the solver.

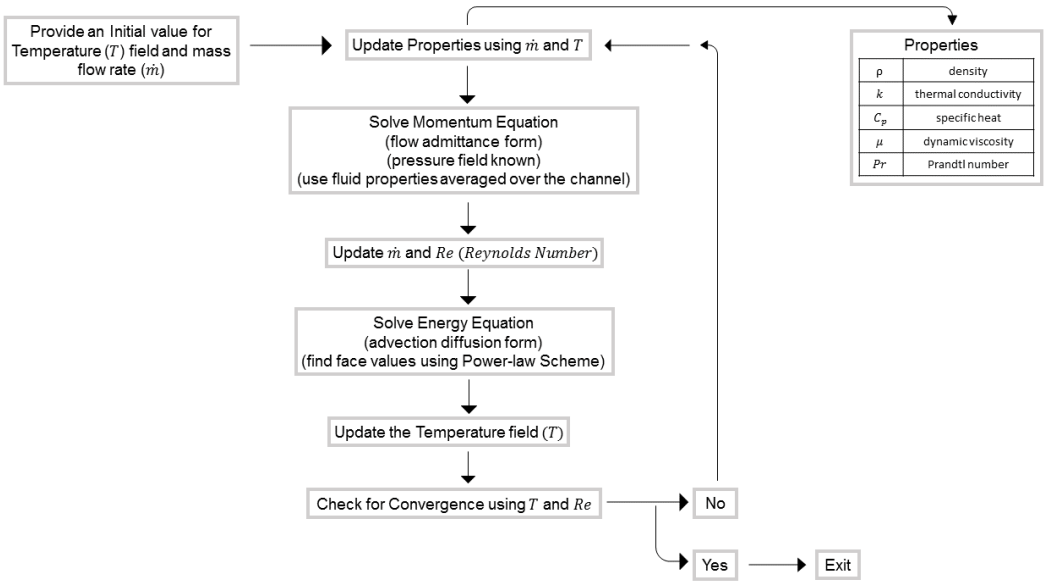

Figure 3-18 Methodology

The convergence criteria is set to 1×10^{-10}. The following flowchart describes basic methodology for solving momentum equation.

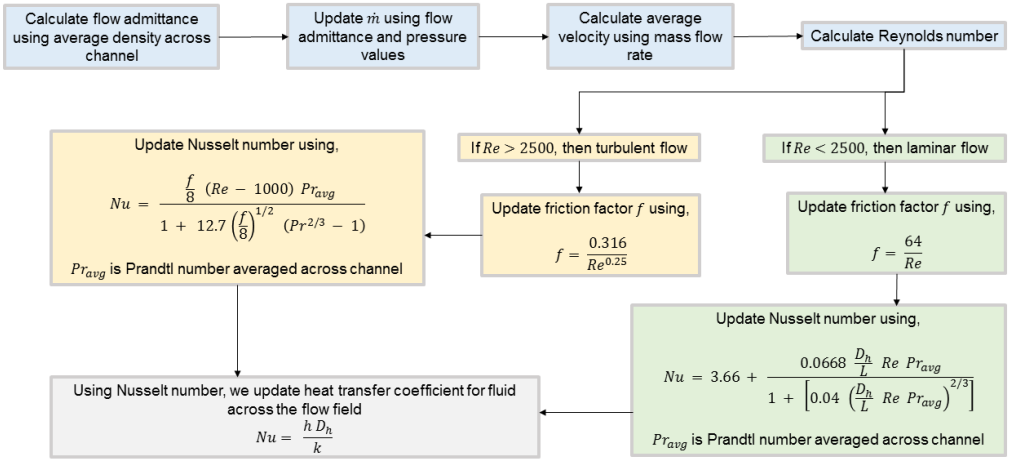

Figure 3-19 Methodology for Momentum Equation

3.4 Model for Fluid Channels

The pressures at inlet and outlet of fluid channels are defined. A linear pressure drop is assumed across the channel. The temperatures at inlet of fluid channels is defined.

Consider the analogy between fluid flow and flow of electric current. We can say that,

$$mass\ flow\ rate\ =\ \frac{pressure\ difference}{flow\ resistance}$$

or,

$$mass\ flow\ rate\ =\ flow\ admittance\ \times\ pressure\ difference$$

General 1-D momentum equation for any flow channel with constant channel area and hydraulic diameter assuming density does not change much, is given as following.

$$\dot{m}_{ch}\ =\ \left[\frac{2}{f}\ \rho_{ch\_avg}\ D_h\ {A_{ch}}^2\ \frac{P_{inlet}\ -\ P_{outlet}}{L}\right]^{0.5} \tag{4}$$

where,

$\rho_{ch\_avg}\ =\ average\ density\ of\ fluid\ in\ channel\ \ (kg/m^3)$

$D_h\ =\ hydraulic\ diameter\ \ (m)$

$A_{ch}\ =\ cross\ sectional\ area\ of\ channel\ (m^2)$

$L\ =\ length\ of\ channel\ (m)$

$P_{inlet}\ =\ pressure\ at\ inlet\ (Pa)$

$P_{outlet}\ =\ pressure\ at\ outlet\ (Pa)$

$f\ =\ friction\ factor\ for\ the\ duct$

$$\dot{m}_{ch}{}^2\ =\ \frac{2}{f}\ \rho_{ch\_avg}\ D_h\ {A_{ch}}^2\ \frac{P_{high}\ -\ P_{low}}{L}$$

We define flow admittance as,

$$\alpha = \frac{2\,\rho_{ch\_avg}\,D_h\,{A_{ch}}^2}{f\,L} \tag{5}$$

Therefore mass flow rate is given by,

$$\dot{m}_{ch} = sqrt\left[\alpha\,(P_{high} - P_{low})\right] \tag{6}$$

Now we calculate average velocity using mass flow rate,

$$\dot{m}_{ch} = \rho_{ch\_avg}\;A_{ch}\;V_{avg}$$

Next we calculate the Reynolds number,

$$Re = \frac{\rho_{ch\_avg}\;V_{avg}\;D_h}{\mu_{avg}}$$

For an internal flow, the flow regime is laminar if $Re < 2500$ and turbulent if $Re \geq 2500$

Hence, if the flow is laminar we substitute,

$$f = \frac{64}{Re}$$

We then find the Nusselt number from following relation [9],

$$Nu = 3.66 + \frac{0.0668\;\frac{D_h}{L}\;Re\;Pr_{avg}}{1 + \left[0.04\;\left(\frac{D_h}{L}\;Re\;Pr_{avg}\right)^{2/3}\right]} \tag{7}$$

where,

$Pr_{avg} = Prandtl\ number\ averaged\ over\ the\ channel$

If the flow is turbulent we substitute,

$$f = \frac{0.316}{Re^{0.25}}$$

We then find the Nusselt number from following relation [9],

$$Nu = \frac{\frac{f}{8}\ (Re - 1000)\ Pr_{avg}}{1 + 12.7\left(\frac{f}{8}\right)^{1/2}\ (Pr^{2/3} - 1)} \tag{8}$$

After Nusselt number is calculated depending on the flow characteristics, we calculate local convective heat transfer coefficient for fluid across flow field using local thermal conductivity and solve energy equation.

$$Nu = \frac{h\ D_h}{k}$$

Consider a single heat exchanger channel with uniform cross section area and heat convection from wall. The one dimensional energy equation neglecting viscous drag is given as following.

$$\rho c_p u \frac{\partial T}{\partial y} = \frac{\partial}{\partial y}\left(k \frac{\partial T}{\partial y}\right) + u \frac{\partial P}{\partial y} + \dot{q}_{to\_channel} \tag{9}$$

where, $\dot{q}_{to\_channel}$ represents the volumetric heat generation and is given by,

$$\dot{q}_{to\_channel} = \frac{hA_{wall}(T_{wall} - T)}{V_{CV}}$$

Now, we can say that,

$$\rho c_p u \frac{\partial T}{\partial y} = \frac{\partial\left(\rho c_p u T\right)}{\partial y} - c_p T \frac{\partial(\rho u)}{\partial y} - \rho u T \frac{\partial c_p}{\partial y}$$

Therefore equation (9) becomes,

$$\frac{\partial\left(\rho c_p u T\right)}{\partial y} - c_p T \frac{\partial(\rho u)}{\partial y} - \rho u T \frac{\partial c_p}{\partial y} = \frac{\partial}{\partial y}\left(k \frac{\partial T}{\partial y}\right) + u \frac{\partial P}{\partial y} + \dot{q}_{to\_channel} \tag{10}$$

Rearranging equation (10)

$$\frac{\partial}{\partial y}\left(\rho c_p u T - k \frac{\partial T}{\partial y}\right) = c_p T \frac{\partial(\rho u)}{\partial y} + \rho u T \frac{\partial c_p}{\partial y} + u \frac{\partial P}{\partial y} + \dot{q}_{to\_channel}$$

(11)

Consider the LHS of equation (11)

$$\frac{\partial}{\partial y}\left(\rho c_p u T - k\frac{\partial T}{\partial y}\right) = \frac{\partial}{\partial y}\left[c_p\left(\rho u T - \frac{k}{c_p}\frac{\partial T}{\partial y}\right)\right]$$

$$= \frac{\partial c_p}{\partial y}\left(\rho u T - \frac{k}{c_p}\frac{\partial T}{\partial y}\right) + c_p\frac{\partial}{\partial y}\left(\rho u T - \frac{k}{c_p}\frac{\partial T}{\partial y}\right)$$

Therefore equation (11) becomes,

$$\frac{\partial c_p}{\partial y}\left(\rho u T - \frac{k}{c_p}\frac{\partial T}{\partial y}\right) + c_p\frac{\partial}{\partial y}\left(\rho u T - \frac{k}{c_p}\frac{\partial T}{\partial y}\right)$$

$$= c_p T\frac{\partial(\rho u)}{\partial y} + \rho u T\frac{\partial c_p}{\partial y} + u\frac{\partial P}{\partial y} + \dot{q}_{to\_channel}$$

Cancelling $\rho u T\frac{\partial c_p}{\partial y}$ from both sides and dividing by c_p,

$$\frac{\partial}{\partial y}\left(\rho u T - \frac{k}{c_p}\frac{\partial T}{\partial y}\right) = T\frac{\partial(\rho u)}{\partial y} + \frac{1}{c_p}u\frac{\partial P}{\partial y} + \frac{1}{c_p}\dot{q}_{to\_channel} + \frac{k}{{c_p}^2}\frac{\partial T}{\partial y}\frac{\partial c_p}{\partial y}$$

We say,

$$\phi = T;\ \Gamma = \frac{k}{c_p};\ S = \frac{1}{c_p}u\frac{\partial P}{\partial y} + \frac{1}{c_p}\dot{q}_{to\_channel} + \frac{k}{{c_p}^2}\frac{\partial T}{\partial y}\frac{\partial c_p}{\partial y}$$

Therefore we get,

$$\frac{\partial}{\partial y}\left(\rho u\phi - \Gamma\frac{\partial\phi}{\partial y}\right) = \phi\frac{\partial(\rho u)}{\partial y} + S$$

(12)

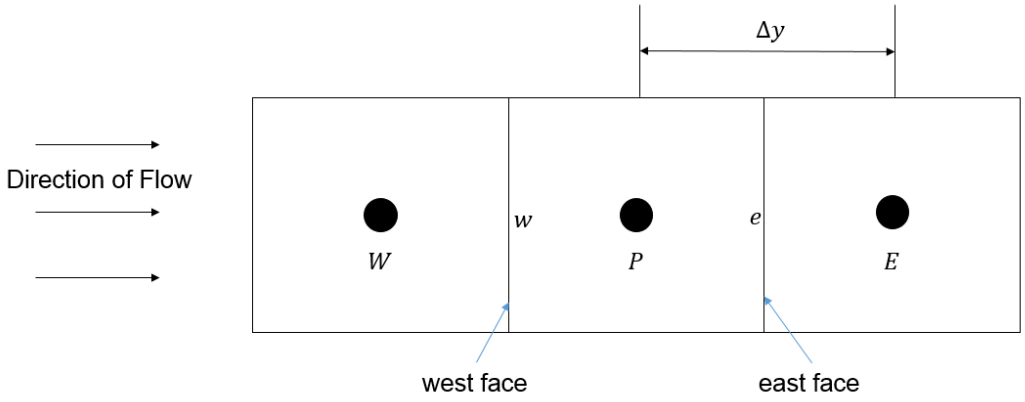

Figure 3-20 Fluid Finite Volume Configuration

We integrate above equation over the finite control volume and apply Gauss divergence theorem to get,

$$\int \frac{\partial}{\partial y}\left(\rho u\phi - \Gamma\frac{\partial \phi}{\partial y}\right) dV = \int \phi \frac{\partial(\rho u)}{\partial y}\, dV + S\,\Delta y\, A_c \tag{13}$$

where A_c is the cross-sectional area of the channel.

Consider,

$$\int \frac{\partial}{\partial y}\left(\rho u\phi - \Gamma\frac{\partial \phi}{\partial y}\right) dV = \int_w^e \left(\rho u\phi - \Gamma\frac{\partial \phi}{\partial y}\right) dA = \left[\left(\rho u\phi - \Gamma\frac{\partial \phi}{\partial y}\right) A_c\right]_w^e$$

$$= \left[\left(\rho u\phi - \Gamma\frac{\partial \phi}{\partial y}\right) A_c\right]_e - \left[\left(\rho u\phi - \Gamma\frac{\partial \phi}{\partial y}\right) A_c\right]_w$$

$$= \left[(\rho u\phi A_c)_e - \left(\Gamma\frac{\partial \phi}{\partial y} A_c\right)_e\right] - \left[(\rho u\phi A_c)_w - \left(\Gamma\frac{\partial \phi}{\partial y} A_c\right)_w\right]$$

Consider,

$$\int \phi \frac{\partial(\rho u)}{\partial y}\, dV = \phi_P \int_w^e \rho u\, dA = \phi_P[\rho u\, A_c]_w^e = \phi_P[\rho u\, A_c]_e - \phi_P[\rho u\, A_c]_w$$

Therefore equation (13) becomes,

$$\left[(\rho u \phi A_c)_e - \left(\Gamma \frac{\partial \phi}{\partial y} A_c\right)_e\right] - \left[(\rho u \phi A_c)_w - \left(\Gamma \frac{\partial \phi}{\partial y} A_c\right)_w\right]$$
$$= \phi_P [\rho u\, A_c]_e - \phi_P [\rho u\, A_c]_w + S\, \Delta y\, A_c \tag{14}$$

$$(\rho u A_c)_e\, \phi_e - (\Gamma A_c)_e \left(\frac{\partial \phi}{\partial y}\right)_e - (\rho u A_c)_w\, \phi_w + (\Gamma A_c)_w \left(\frac{\partial \phi}{\partial y}\right)_w$$
$$= \phi_P (\rho u A_c)_e - \phi_P (\rho u A_c)_w + S\, \Delta y\, A_c \tag{15}$$

Now,

The value of ϕ on east face is given by,

$$\phi_e = \frac{\phi_P + \phi_E}{2}$$

The value of ϕ on west face is given by,

$$\phi_w = \frac{\phi_W + \phi_P}{2}$$

The change in ϕ with respect to y, on east face is given by,

$$\left(\frac{\partial \phi}{\partial y}\right)_e = \frac{\phi_E - \phi_P}{\Delta y}$$

The change in ϕ with respect to y, on west face is given by,

$$\left(\frac{\partial \phi}{\partial y}\right)_w = \frac{\phi_P - \phi_W}{\Delta y}$$

Therefore equation (15) becomes,

$$(\rho u A_c)_e \frac{\phi_P + \phi_E}{2} - (\Gamma A_c)_e \frac{\phi_E - \phi_P}{\Delta y} - (\rho u A_c)_w \frac{\phi_W + \phi_P}{2} + (\Gamma A_c)_w \frac{\phi_P - \phi_W}{\Delta y}$$
$$= \phi_P (\rho u A_c)_e - \phi_P (\rho u A_c)_w + S\, \Delta y\, A_c \tag{16}$$

$$\frac{(\rho u A_c)_e}{2}\,\phi_P + \frac{(\rho u A_c)_e}{2}\,\phi_E - \left(\frac{\Gamma A_c}{\Delta y}\right)_e \phi_E + \left(\frac{\Gamma A_c}{\Delta y}\right)_e \phi_P - \frac{(\rho u A_c)_w}{2}\,\phi_W - \frac{(\rho u A_c)_w}{2}\,\phi_P + \left(\frac{\Gamma A_c}{\Delta y}\right)_w \phi_P - \left(\frac{\Gamma A_c}{\Delta y}\right)_w \phi_W = \phi_P(\rho u A_c)_e - \phi_P(\rho u A_c)_w + S\,\Delta y\,A_c \tag{17}$$

Consider the 'S' term,

$$S = \frac{1}{c_p} u \frac{\partial P}{\partial y} + \frac{1}{c_p}\dot{q}_{to\_channel} + \frac{k}{{c_p}^2}\frac{\partial T}{\partial y}\frac{\partial c_p}{\partial y} = \frac{1}{c_p}\left[u\frac{\partial P}{\partial y} + \dot{q}_{to\_channel} + \frac{k}{c_p}\frac{\partial T}{\partial y}\frac{\partial c_p}{\partial y}\right] = \frac{1}{c_p}\left[u\frac{\Delta P}{\Delta y} + \dot{q}_{to\_channel} + \frac{k}{c_p}\frac{\Delta \phi}{\Delta y}\frac{\Delta c_p}{\Delta y}\right] \tag{18}$$

We model the $\dot{q}_{to\_channel}$ term as,

$$\dot{q}_{to\_channel} = \frac{h_{fluid}\,A_{conv\_mid\_plate}\,(\phi_{middle\_plate} - \phi_{fluid})}{\Delta y\,A_c} + \frac{h_{fluid}\,A_{conv\_fin}\,(\phi_{fin\_right} - \phi_{fluid})}{\Delta y\,A_c} + \frac{h_{fluid}\,A_{conv\_fin}\,(\phi_{fin\_left} - \phi_{fluid})}{\Delta y\,A_c}$$

Units of $\dot{q}_{to\_channel}$ term are W/m^3. Energy interaction between corresponding finite volumes of fluid, middle plate and fins is modelled in the source term. This is indicative that any given finite volume of fluid interacts with fins on both sides and middle plate. In case of the fluid finite volumes at edges, fluid will interact with fin only on one side and with wall on other side. The fluid shares an adiabatic condition with wall. Therefore from equation (18) we get,

$$S = \frac{1}{c_p}\left[u\frac{\Delta P}{\Delta y} + \frac{h_{fluid}\,A_{conv\_mid\_plate}\,(\phi_{mid\_plate} - \phi_P)}{\Delta y\,A_c}\right.$$

$$+ \frac{h_{fluid}\,A_{conv\_fin}\,(\phi_{fin\_right} - \phi_P)}{\Delta y\,A_c} + \frac{h_{fluid}\,A_{conv\_fin}\,(\phi_{fin\_left} - \phi_P)}{\Delta y\,A_c}$$

$$\left. + \frac{k}{c_p}\frac{\Delta\phi}{\Delta y}\frac{\Delta c_p}{\Delta y}\right]$$

Therefore, consider the last term from equation (14)

$$S\,\Delta y\,A_c = \frac{1}{c_p}\left[u\frac{\Delta P}{\Delta y} + \frac{h_{fluid}\,A_{conv\_mid\_plate}\,(\phi_{mid\_plate} - \phi_P)}{\Delta y\,A_c}\right.$$

$$+ \frac{h_{fluid}\,A_{conv\_fin}\,(\phi_{fin\_right} - \phi_P)}{\Delta y\,A_c} + \frac{h_{fluid}\,A_{conv\_fin}\,(\phi_{fin\_left} - \phi_P)}{\Delta y\,A_c}$$

$$\left. + \frac{k}{c_p}\frac{\Delta\phi}{\Delta y}\frac{\Delta c_p}{\Delta y}\right]\Delta y\,A_c$$

$$= \frac{u}{c_p}\Delta P A_c + \frac{h_{fluid}\,A_{conv\_mid\_plate}\,(\phi_{mid\_plate} - \phi_P)}{c_p}$$

$$+ \frac{h_{fluid}\,A_{conv\_fin}\,(\phi_{fin\_right} - \phi_P)}{c_p} + \frac{h_{fluid}\,A_{conv\_fin}\,(\phi_{fin\_left} - \phi_P)}{c_p}$$

$$+ \frac{k}{{c_p}^2}\frac{\Delta\phi}{\Delta y}\Delta c_p A_c$$

Therefore equation (14) becomes,

$$\frac{(\rho u A_c)_e}{2}\,\phi_P + \frac{(\rho u A_c)_e}{2}\,\phi_E - \left(\frac{\Gamma A_c}{\Delta y}\right)_e \phi_E + \left(\frac{\Gamma A_c}{\Delta y}\right)_e \phi_P - \frac{(\rho u A_c)_w}{2}\,\phi_W - \frac{(\rho u A_c)_w}{2}\,\phi_P$$

$$+ \left(\frac{\Gamma A_c}{\Delta y}\right)_w \phi_P - \left(\frac{\Gamma A_c}{\Delta y}\right)_w \phi_W$$

$$= \phi_P(\rho u A_c)_e - \phi_P(\rho u A_c)_w + \frac{u}{c_p}\Delta P A_c$$

$$+ \frac{h_{fluid}\, A_{conv\_mid\_plate}\,(\phi_{mid\_plate} - \phi_P)}{c_p}$$

$$+ \frac{h_{fluid}\, A_{conv\_fin}\,(\phi_{fin\_right} - \phi_P)}{c_p} + \frac{h_{fluid}\, A_{conv\_fin}\,(\phi_{fin\_left} - \phi_P)}{c_p}$$

$$+ \frac{k}{{c_p}^2}\frac{\Delta\phi}{\Delta y}\Delta c_p A_c$$

(19)

Now we define the following,

Convection factors:

$$F_e = (\rho u)_e\, A_c$$

$$F_w = (\rho u)_w\, A_c$$

Diffusion factors:

$$D_e = \left(\frac{\Gamma}{\Delta y}\right)_e A_c$$

$$D_w = \left(\frac{\Gamma}{\Delta y}\right)_w A_c$$

Therefore equation (19) becomes,

$$\frac{F_e}{2}\,\phi_P + \frac{F_e}{2}\,\phi_E - D_e\,\phi_E + D_e\,\phi_P - \frac{F_w}{2}\,\phi_W - \frac{F_w}{2}\,\phi_P + D_w\,\phi_P - D_w\,\phi_W$$
$$= F_e\,\phi_P - F_w\,\phi_P + \frac{u}{c_p}\Delta P A_c + \frac{h_{fluid}\,A_{conv\_mid\_plate}}{c_p}\phi_{mid\_plate}$$
$$- \frac{h_{fluid}\,A_{conv\_mid\_plate}}{c_p}\phi_P + \frac{h_{fluid}\,A_{conv\_fin}}{c_p}\phi_{fin\_right}$$
$$- \frac{h_{fluid}\,A_{conv\_fin}}{c_p}\phi_P + \frac{h_{fluid}\,A_{conv\_fin}}{c_p}\phi_{fin\_left} - \frac{h_{fluid}\,A_{conv\_fin}}{c_p}\phi_P$$
$$+ \frac{k}{{c_p}^2}\frac{\Delta\phi}{\Delta y}\Delta c_p A_c$$

(20)

$$\left[-\frac{F_e}{2} + D_e + \frac{F_w}{2} + D_w + \frac{h_{fluid}\,A_{conv\_mid\_plate}}{c_p} + \frac{h_{fluid}\,A_{conv\_fin}}{c_p} + \frac{h_{fluid}\,A_{conv\_fin}}{c_p}\right]\phi_P$$
$$= \left[-\frac{F_e}{2} + D_e\right]\phi_E + \left[\frac{F_w}{2} + D_w\right]\phi_W + \frac{h_{fluid}\,A_{conv\_mid\_plate}}{c_p}\phi_{mid\_plate}$$
$$+ \frac{h_{fluid}\,A_{conv\_fin}}{c_p}\phi_{fin\_right} + \frac{h_{fluid}\,A_{conv\_fin}}{c_p}\phi_{fin\_left} + \frac{u}{c_p}\Delta P A_c$$
$$+ \frac{k}{{c_p}^2}\frac{\Delta\phi}{\Delta y}\Delta c_p A_c$$

(21)

Therefore we can say that,

$$a_P\phi_P = a_E\phi_E + a_W\phi_W + a_{mid\_plate}\phi_{mid\_plate} + a_{fin\_right}\phi_{fin\_right} + a_{fin\_left}\phi_{fin\_left} + b$$

Where,

$$a_P = -\frac{F_e}{2} + D_e + \frac{F_w}{2} + D_w + \frac{h_{fluid}\,A_{conv\_mid\_plate}}{c_p} + \frac{h_{fluid}\,A_{conv\_fin}}{c_p} + \frac{h_{fluid}\,A_{conv\_fin}}{c_p}$$

$$a_E = -\frac{F_e}{2} + D_e$$

$$a_W = \frac{F_w}{2} + D_w$$

$$a_{mid\_plate} = \frac{h_{fluid}\, A_{conv\_mid\_plate}}{c_p}$$

$$a_{fin\_right} = \frac{h_{fluid}\, A_{conv\_fin}}{c_p}$$

$$a_{fin\_left} = \frac{h_{fluid}\, A_{conv\_fin}}{c_p}$$

$$b = \frac{u}{c_p}\Delta P A_c + \frac{k}{{c_p}^2}\frac{\Delta\phi}{\Delta y}\Delta c_p A_c$$

Therefore,

$$a_P = a_E + a_W + a_{mid\_plate} + a_{fin\_right} + a_{fin\_left}$$

Peclet number is defined as the ratio of convection factor to diffusion factor. It is a dimensionless number which determines whether convection or diffusion physics dominates the problem. The higher the magnitude of Pe, the greater is the effect of convective transport.

Therefore,

$$a_E = D_e(1 - 0.5Pe_e)$$

$$a_W = D_w(1 - 0.5Pe_w)$$

Now, using power law scheme, we update the coefficients.

$$a_W = D_W[\![0, (1 - 0.1|Pe_w|)^5]\!] + [\![F_w, 0]\!]$$

$$a_E = D_E[\![0, (1 - 0.1|Pe_e|)^5]\!] + [\![F_E, 0]\!]$$

According to above scheme, if Pe will be equal to or greater than 10, diffusion will be ignored. Therefore using these coefficients we solve iteratively for ϕ_P (T_{fluid}).

3.4 Model for Middle Plate

Consider 2D Diffusion equation with source.

$$\frac{\partial}{\partial x}\left[k\frac{\partial T}{\partial x}\right] + \frac{\partial}{\partial y}\left[k\frac{\partial T}{\partial y}\right] + \ddot{q}_{to\_middle\_plate} = 0$$

$\ddot{q}_{to\_middle\_plate}$ is the volumetric heat generation (W/m^3).

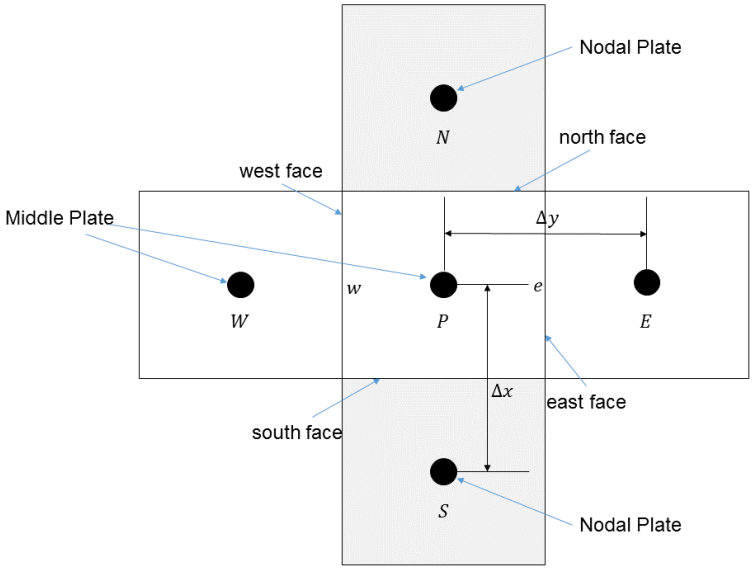

Figure 3-21 Middle Plate Finite Volume Configuration

Integrating above equation over the finite volume, we get.

$$\int_s^n \frac{\partial}{\partial x}\left[k\frac{\partial T}{\partial x}\right]dx + \int_w^e \frac{\partial}{\partial y}\left[k\frac{\partial T}{\partial y}\right]dy + \{\ddot{q}_{to\_middle\_plate} * (dx * dy * plate_{thickness})\} = 0 \quad (22)$$

Applying Gauss Divergence theorem, we get.

$$\int_s^n \left[k\frac{\partial T}{\partial x}\right]dA + \int_w^e \left[k\frac{\partial T}{\partial y}\right]dA + \dot{q}_{to\_middle\_plate} = 0$$

We model the $\dot{q}_{to\_middle\_plate}$ term as,

$$\dot{q}_{to\_middle\_plate} = h_{hot\_fluid}\, A_{conv\_mid\_plate} \left(\phi_{hot\_fluid} - \phi_{middle\_plate}\right) - h_{cold\_fluid}\, A_{conv\_mid\_plate} \left(\phi_{middle\_plate} - \phi_{cold\_fluid}\right)$$

According to formulation, energy is transferred from finite volume of hot fluid to the corresponding finite volume of middle plate and from middle plate to cold fluid.

$$\left[kA_{c/s\_P}\frac{\partial T}{\partial x}\right]_n - \left[kA_{c/s\_P}\frac{\partial T}{\partial x}\right]_s + \left[kA_{c/s\_P}\frac{\partial T}{\partial y}\right]_e - \left[kA_{c/s\_P}\frac{\partial T}{\partial y}\right]_w + \left[\left\{h_{hf} * A_{conv\_mid\_plate} * (T_{hf} - T_P)\right\} - \left\{h_{cf} * A_{conv\_mid\_plate} * \left(T_P - T_{cf}\right)\right\}\right] = 0 \quad (23)$$

where A_{c/s_P} is the cross-sectional area of the middle plate.

$$k_n A_{c/s\_P_n}\frac{T_N - T_P}{\Delta x} - k_s A_{c/s\_P_s}\frac{T_P - T_S}{\Delta x} + k_e A_{c/s\_P_e}\frac{T_E - T_P}{\Delta y} - k_w A_{c/s\_P_w}\frac{T_P - T_W}{\Delta y} + \left\{h_{hf} * A_{conv\_mid\_plate} * (T_{hf} - T_P)\right\} - \left\{h_{cf} * A_{conv\_mid\_plate} * \left(T_P - T_{cf}\right)\right\} = 0 \quad (24)$$

$$\left[\frac{k_n A_{c/s\_P_n}}{\Delta x} + \frac{k_s A_{c/s\_P_s}}{\Delta x} + \frac{k_e A_{c/s\_P_e}}{\Delta y} + \frac{k_w A_{c/s\_P_w}}{\Delta y} + h_{hf} A_{conv\_mid\_plate} + h_{cf} A_{conv\_mid\_plate}\right] T_P = \frac{k_n A_{c/s\_P_n}}{\Delta x} T_N + \frac{k_s A_{c/s\_P_s}}{\Delta x} T_S + \frac{k_e A_{c/s\_P_e}}{\Delta y} T_E + \frac{k_w A_{c/s\_P_w}}{\Delta y} T_W + h_{hf} A_{conv\_mid\_plate} T_{hf} + h_{cf} A_{conv\_mid\_plate} T_{cf} \quad (25)$$

Now we say,

$$a_P T_P = a_N T_N + a_S T_S + a_E T_E + a_W T_W + b_{hf} T_{hf} + b_{cf} T_{cf}$$

Where,

$$a_N = \frac{k_n A_{c/s\_P_n}}{\Delta x}$$

$$a_S = \frac{k_s A_{c/s\_P_s}}{\Delta x}$$

$$a_E = \frac{k_e A_{c/s\_P_e}}{\Delta y}$$

$$a_W = \frac{k_w A_{c/s\_P_w}}{\Delta y}$$

$$b_{hf} = h_{hf} A_{conv\_mid\_plate}$$

$$b_{cf} = h_{cf} A_{conv\_mid\_plate}$$

$$a_P = \frac{k_n A_{c/s_n}}{\Delta x} + \frac{k_s A_{c/s_s}}{\Delta x} + \frac{k_e A_{c/s_e}}{\Delta y} + \frac{k_w A_{c/s_w}}{\Delta y} + h_{hf} A_{conv\_mid\_plate} + h_{cf} A_{conv\_mid\_plate}$$

Hence we can say that,

$$a_P = a_N + a_S + a_E + a_W + b_{hf} + b_{cf}$$

We solve iteratively for T_{middle_plate}.

3.5 Model for Nodal Plate

Consider 2D Diffusion equation with source.

$$\frac{\partial}{\partial x}\left[k\frac{\partial T}{\partial x}\right] + \frac{\partial}{\partial y}\left[k\frac{\partial T}{\partial y}\right] + \ddot{q}_{to\_nodal\_plate} = 0$$

$\ddot{q}_{to\_nodal\_plate}$ is the volumetric heat generation (W/m^3).

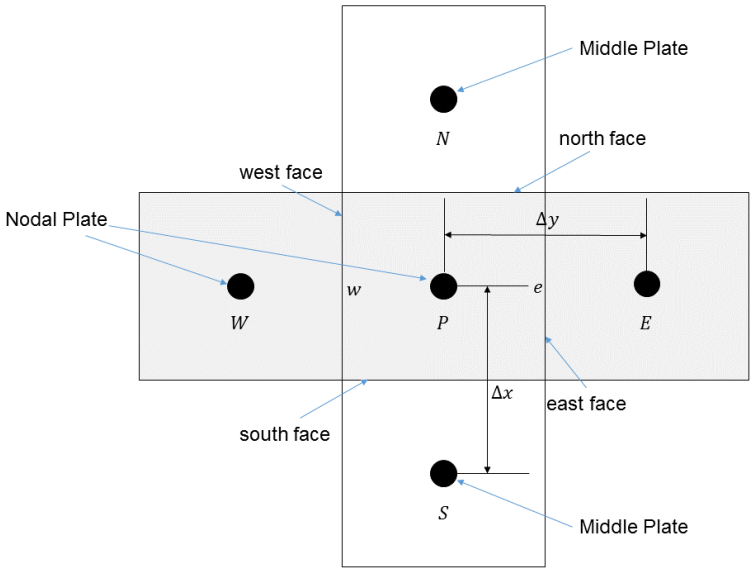

Figure 3-22 Nodal Plate Finite Volume Configuration

Integrating the above equation over the finite volume, we get.

$$\int_{s}^{n} \frac{\partial}{\partial x}\left[k\frac{\partial T}{\partial x}\right]dx \;+\; \int_{w}^{e} \frac{\partial}{\partial y}\left[k\frac{\partial T}{\partial y}\right]dy \;+\; \{\ddot{q}_{to\_nodal\_plate} * (dx * dy * plate_{thickness})\} \;=\; 0 \tag{26}$$

Applying Gauss Divergence theorem, we get.

$$\int_{s}^{n} \left[k\frac{\partial T}{\partial x}\right]dA \;+\; \int_{w}^{e} \left[k\frac{\partial T}{\partial y}\right]dA \;+\; \dot{q}_{to\_nodal\_plate} \;=\; 0$$

Now,

$$A_{c/s\_nodal\_plate} \;=\; A_{c/s\_P}$$

$$k_{nodal\_plate} \;=\; k_{middle\_plate}$$

We model the $\dot{q}_{to\_nodal\_plate}$ term as,

$$\dot{q}_{to\_nodal\_plate} = \{k_{fin} * A_{c/s\_hor\_fin} * (T_{hot\_fin\_r} - T_{nodal\_plate}) / (0.5 * l_{lat\_fin})\} + \{k_{fin} * A_{c/s\_hor\_fin} * (T_{hot\_fin\_l} - T_{nodal\_plate}) / (0.5 * l_{lat\_fin})\} - \{k_{fin} * A_{c/s\_hor\_fin} * (T_{nodal\_plate} - T_{cold\_fin\_r}) / (0.5 * l_{lat\_fin})\} - \{k_{fin} * A_{c/s\_hor\_fin} * (T_{nodal\_plate} - T_{cold\_fin\_l}) / (0.5 * l_{lat\_fin})\} \quad (27)$$

According to formulation, heat is conducted from hot fins to nodal plate and from the nodal plate to cold fins.

$$\left[kA_{c/s\_P}\frac{\partial T}{\partial x}\right]_n - \left[kA_{c/s\_P}\frac{\partial T}{\partial x}\right]_s + \left[kA_{c/s\_P}\frac{\partial T}{\partial y}\right]_e - \left[kA_{c/s\_P}\frac{\partial T}{\partial y}\right]_w + [\{k_{fin} * A_{c/s\_hor\_fin} * (T_{hot\_fin\_r} - T_{nodal\_plate}) / (0.5 * l_{lat\_fin})\} + \{k_{fin} * A_{c/s\_hor\_fin} * (T_{hot\_fin\_l} - T_{nodal\_plate}) / (0.5 * l_{lat\_fin})\} - \{k_{fin} * A_{c/s\_hor\_fin} * (T_{nodal\_plate} - T_{cold\_fin\_r}) / (0.5 * l_{lat\_fin})\} - \{k_{fin} * A_{c/s\_hor\_fin} * (T_{nodal\_plate} - T_{cold\_fin\_l}) / (0.5 * l_{lat\_fin})\}] = 0 \quad (28)$$

$$k_n A_{c/s\_P_n}\frac{T_N - T_P}{\Delta x} - k_s A_{c/s\_P_s}\frac{T_P - T_S}{\Delta x} + k_e A_{c/s\_P_e}\frac{T_E - T_P}{\Delta y} - k_w A_{c/s\_P_w}\frac{T_P - T_W}{\Delta y} + [\{k_{fin} * A_{c/s\_hor\_fin} * (T_{hot\_fin\_r} - T_P) / (0.5 * l_{lat\_fin})\} + \{k_{fin} * A_{c/s\_hor\_fin} * (T_{hot\_fin\_l} - T_P) / (0.5 * l_{lat\_fin})\} - \{k_{fin} * A_{c/s\_hor\_fin} * (T_P - T_{cold\_fin\_r}) / (0.5 * l_{lat\_fin})\} - \{k_{fin} * A_{c/s\_hor\_fin} * (T_P - T_{cold\_fin\_l}) / (0.5 * l_{lat\_fin})\}] = 0 \quad (29)$$

$$\left[\frac{k_n A_{c/s\_P_n}}{\Delta x} + \frac{k_s A_{c/s\_P_s}}{\Delta x} + \frac{k_e A_{c/s\_P_e}}{\Delta y} + \frac{k_w A_{c/s\_P_w}}{\Delta y} + \frac{k_{fin}\, A_{c/s\_hor\_fin}}{0.5 * l_{lat\_fin}}\right.$$

$$\left. + \frac{k_{fin}\, A_{c/s\_hor\_fin}}{0.5 * l_{lat\_fin}} + \frac{k_{fin}\, A_{c/s\_hor\_fin}}{0.5 * l_{lat\_fin}} + \frac{k_{fin}\, A_{c/s\_hor\_fin}}{0.5 * l_{lat\_fin}}\right] T_P$$

$$= \frac{k_n A_{c/s\_P_n}}{\Delta x} T_N + \frac{k_s A_{c/s\_P_s}}{\Delta x} T_S + \frac{k_e A_{c/s\_P_e}}{\Delta y} T_E + \frac{k_w A_{c/s\_P_w}}{\Delta y} T_W$$

$$+ \frac{k_{fin}\, A_{c/s\_hor\_fin}}{0.5 * l_{lat\_fin}} T_{hot\_fin\_r} + \frac{k_{fin}\, A_{c/s\_hor\_fin}}{0.5 * l_{lat\_fin}} T_{hot\_fin\_l}$$

$$+ \frac{k_{fin}\, A_{c/s\_hor\_fin}}{0.5 * l_{lat\_fin}} T_{cold\_fin\_r} + \frac{k_{fin}\, A_{c/s\_hor\_fin}}{0.5 * l_{lat\_fin}} T_{cold\_fin\_l} \quad (30)$$

Now we say,

$$a_P T_P = a_N T_N + a_S T_S + a_E T_E + a_W T_W + b_{hot\_fin} T_{hot\_fin\_r} + b_{hot\_fin} T_{hot\_fin\_l}$$

$$+ b_{cold\_fin} T_{cold\_fin\_r} + b_{cold\_fin} T_{cold\_fin\_l}$$

Where,

$$a_N = \frac{k_n A_{c/s\_P_n}}{\Delta x}$$

$$a_S = \frac{k_s A_{c/s\_P_s}}{\Delta x}$$

$$a_E = \frac{k_e A_{c/s\_P_e}}{\Delta y}$$

$$a_W = \frac{k_w A_{c/s\_P_w}}{\Delta y}$$

$$b_{hot\_fin} = \frac{k_{fin}\, A_{c/s\_hor\_fin}}{0.5 * l_{lat\_fin}}$$

$$b_{cold\_fin} = \frac{k_{fin}\, A_{c/s\_hor\_fin}}{0.5 * l_{lat\_fin}}$$

$$a_P = \frac{k_n A_{c/s\_P_n}}{\Delta x} + \frac{k_s A_{c/s\_P_s}}{\Delta x} + \frac{k_e A_{c/s\_P_e}}{\Delta y} + \frac{k_w A_{c/s\_P_w}}{\Delta y} + \frac{k_{fin}\, A_{c/s\_hor\_fin}}{0.5 * l_{lat\_fin}}$$

$$+ \frac{k_{fin}\, A_{c/s\_hor\_fin}}{0.5 * l_{lat\_fin}} + \frac{k_{fin}\, A_{c/s\_hor\_fin}}{0.5 * l_{lat\_fin}} + \frac{k_{fin}\, A_{c/s\_hor\_fin}}{0.5 * l_{lat\_fin}}$$

Hence we can say that,

$$a_P = a_N + a_S + a_E + a_W + b_{hot\_fin} + b_{cold\_fin}$$

We solve iteratively for T_{nodal_plate}.

3.6 Model for Fins

Consider the 1D Diffusion equation with source.

$$\frac{\partial}{\partial y}\left[k \frac{\partial T}{\partial y}\right] + \ddot{q}_{to\_fin} = 0$$

$\ddot{q}_{to\_fin}$ is the volumetric heat generation (W/m^3).

Integrating the above equation over the finite volume, we get.

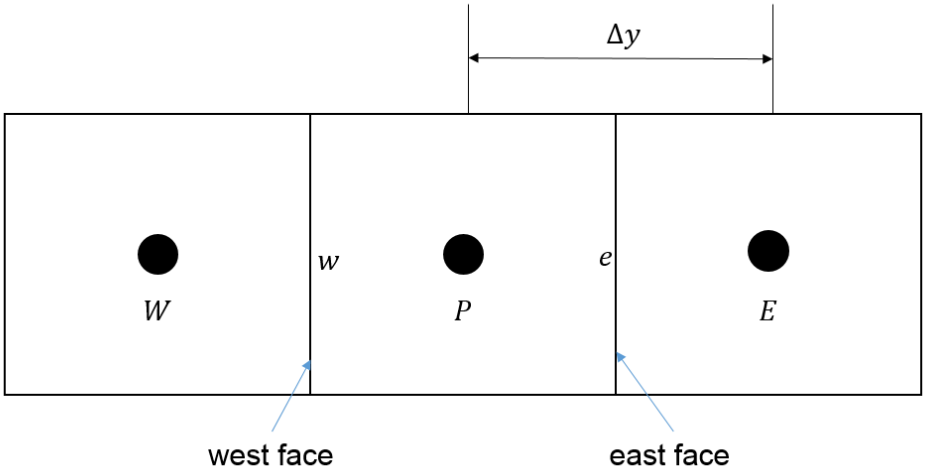

Figure 3-23 Fin Finite Volume Configuration

$$\int_w^e \frac{\partial}{\partial y}\left[k \frac{\partial T}{\partial y}\right] dy + \{\ddot{q}_{to\_fin} * (dy * l_{lat\_fin} * fin_{thickness})\} = 0 \quad (31)$$

Applying Gauss Divergence theorem, we get.

$$\int_{w}^{e} \left[k \frac{\partial T}{\partial y} \right] dA \; + \; \dot{q}_{to\_fin} \; = \; 0$$

Now,

$$A_{c/s\_fin} \; = \; l_{lat\_fin} * fin_{thickness}$$

We model the $\dot{q}_{to\_fin}$ term as,

$$\begin{aligned} \dot{q}_{to\_fin} \; = \; & h_{fluid} \, A_{conv\_fin} \left(T_{fluid\_right} - \; T_{fin} \right) \; + \; h_{fluid} \, A_{conv\_fin} \left(T_{fluid\_left} - \; T_{fin} \right) \\ & - \left\{ k_{fin} * \; A_{c/s\_hor\_fin} * \left(T_{fin} - \; T_{nodal\_plate\_1} \right) / \left(0.5 * \; l_{lat\_fin} \right) \right\} \\ & - \left\{ k_{fin} * \; A_{c/s\_hor\_fin} * \left(T_{fin} - \; T_{nodal\_plate\_2} \right) / \left(0.5 * \; l_{lat\_fin} \right) \right\} \end{aligned} \tag{32}$$

According to formulation, finite volume of fin absorbs heat from hot fluid on both sides and rejects heat to the nodal plates on top and bottom. This is true for hot fins, but the direction of energy transfer will be reversed for cold fins.

$$\begin{aligned} & \left[k A_{c/s\_fin} \frac{\partial T}{\partial y} \right]_{e} \; - \; \left[k A_{c/s\_fin} \frac{\partial T}{\partial y} \right]_{w} \; + \; h_{fluid} \, A_{conv\_fin} \left(T_{fluid\_right} - \; T_{P} \right) \\ & + \; h_{fluid} \, A_{conv\_fin} \left(T_{fluid\_left} - \; T_{P} \right) \\ & - \left\{ k_{fin} * \; A_{c/s\_hor\_fin} * \left(T_{P} - \; T_{nodal\_plate\_1} \right) / \left(0.5 * \; l_{lat\_fin} \right) \right\} \\ & - \left\{ k_{fin} * \; A_{c/s\_hor\_fin} * \left(T_{P} - \; T_{nodal\_plate\_2} \right) / \left(0.5 * \; l_{lat\_fin} \right) \right\} \; = \; 0 \end{aligned} \tag{33}$$

$$\begin{aligned} & k_{e} A_{c/s\_fin} \frac{T_{E} - \; T_{P}}{\Delta y} \; - \; k_{w} A_{c/s\_fin} \frac{T_{P} - \; T_{W}}{\Delta y} \; + \; h_{fluid} \, A_{conv\_fin} \left(T_{fluid\_right} - \; T_{P} \right) \\ & + \; h_{fluid} \, A_{conv\_fin} \left(T_{fluid\_left} - \; T_{P} \right) \\ & - \left\{ k_{fin} * \; A_{c/s\_hor\_fin} * \left(T_{P} - \; T_{nodal\_plate\_1} \right) / \left(0.5 * \; l_{lat\_fin} \right) \right\} \\ & - \left\{ k_{fin} * \; A_{c/s\_hor\_fin} * \left(T_{P} - \; T_{nodal\_plate\_2} \right) / \left(0.5 * \; l_{lat\_fin} \right) \right\} \; = \; 0 \end{aligned} \tag{34}$$

$$\left[\frac{k_e A_{c/s\_fin}}{\Delta y} + \frac{k_w A_{c/s\_fin}}{\Delta y} + h_{fluid}\, A_{conv\_fin} + h_{fluid}\, A_{conv\_fin} + \frac{k_{fin}\, A_{c/s\_hor\_fin}}{0.5 * l_{lat\_fin}} + \frac{k_{fin}\, A_{c/s\_hor\_fin}}{0.5 * l_{lat\_fin}}\right] T_P$$

$$= \frac{k_e A_{c/s\_fin}}{\Delta y} T_E + \frac{k_w A_{c/s\_fin}}{\Delta y} T_W + h_{fluid}\, A_{conv\_fin}\, T_{fluid\_right} + h_{fluid}\, A_{conv\_fin}\, T_{fluid\_left} + \frac{k_{fin}\, A_{c/s\_hor\_fin}}{0.5 * l_{lat\_fin}} T_{nodal\_plate\_1} + \frac{k_{fin}\, A_{c/s\_hor\_fin}}{0.5 * l_{lat\_fin}} T_{nodal\_plate\_2} \quad (35)$$

Now we say,

$$a_P\, T_P = a_E T_E + a_W T_W + b_{fluid\_right} T_{fluid\_right} + b_{fluid\_left} T_{fluid\_left} + b_{nodal\_plate\_1} T_{nodal\_plate\_1} + b_{nodal\_plate\_2} T_{nodal\_plate\_2}$$

Where,

$$a_E = \frac{k_e A_{c/s\_fin}}{\Delta y}$$

$$a_W = \frac{k_w A_{c/s\_fin}}{\Delta y}$$

$$b_{fluid\_right} = h_{fluid}\, A_{conv\_fin}$$

$$b_{fluid\_left} = h_{fluid}\, A_{conv\_fin}$$

$$b_{nodal\_plate\_1} = \frac{k_{fin}\, A_{c/s\_hor\_fin}}{0.5 * l_{lat\_fin}}$$

$$b_{nodal\_plate\_2} = \frac{k_{fin}\, A_{c/s\_hor\_fin}}{0.5 * l_{lat\_fin}}$$

$$a_P = \frac{k_e A_{c/s\_fin}}{\Delta y} + \frac{k_w A_{c/s\_fin}}{\Delta y} + h_{fluid}\, A_{conv\_fin} + h_{fluid}\, A_{conv\_fin} + \frac{k_{fin}\, A_{c/s\_hor\_fin}}{0.5 * l_{lat\_fin}}$$

$$+ \frac{k_{fin}\, A_{c/s\_hor\_fin}}{0.5 * l_{lat\_fin}}$$

Hence we can say that,

$$a_P = a_E + a_W + b_{fluid\_right} + b_{fluid\_left} + b_{nodal\_plate\_1} + b_{nodal\_plate\_2}$$

We solve iteratively for T_{fin}.

Chapter 4

RESULTS AND DISCUSSIONS

4.1 Verification of Numerical Model

The numerical accuracy of model can be examined by verifying that the predicted heat transfer rates satisfy first law from a global standpoint and also from a local standpoint for every finite volume. An energy balance on an arbitrary finite volume in the model should satisfy the balance equation.

Energy balance for hot fluid finite volume:

$$enthalpy_{in} - heat\ interaction_{middle\ plate} - heat\ interaction_{hot\ fin} - enthalpy_{out} = 0 \quad (36)$$

Energy balance for cold fluid finite volume:

$$enthalpy_{in} + heat\ interaction_{middle\ plate} + heat\ interaction_{cold\ fin} - enthalpy_{out} = 0 \quad (37)$$

Energy balance for middle plate finite volume:

$$heat\ interaction_{hot\ fluid} - heat\ conduction_{middle\ plate} - heat\ conduction_{nodal\ plate} - heat\ interaction_{cold\ fluid} = 0 \quad (38)$$

Energy balance for nodal plate finite volume:

$$heat\ conduction_{hot\ fin} + heat\ conduction_{nodal\ plate} + heat\ conduction_{middle\ plate} - heat\ conduction_{cold\ fin} = 0 \quad (39)$$

Energy balance for hot fin finite volume:

$$heat\ interaction_{hot\ fluid} - heat\ conduction_{hot\ fin} - heat\ conduction_{nodal\ plate} = 0 \quad (40)$$

Energy balance for cold fin finite volume:

$$heat\ conduction_{nodal\ plate} + heat\ conduction_{cold\ fin} - heat\ interaction_{cold\ fluid} = 0 \quad (41)$$

Equations (36), (37), (38), (39), (40) and (41) are satisfied to numerical accuracy under arbitrary conditions.

The analytical solution for heat exchanger effectiveness in terms of NTU for a counter-flow heat exchanger is given as [9],

$$\varepsilon = \frac{1 - exp[-NTU\ (1 - C_r)]}{1 - C_r\ exp[-NTU\ (1 - C_r)]}, \qquad (C_r < 1)$$

$$\varepsilon = \frac{NTU}{1 + NTU}, \qquad (C_r = 1)$$

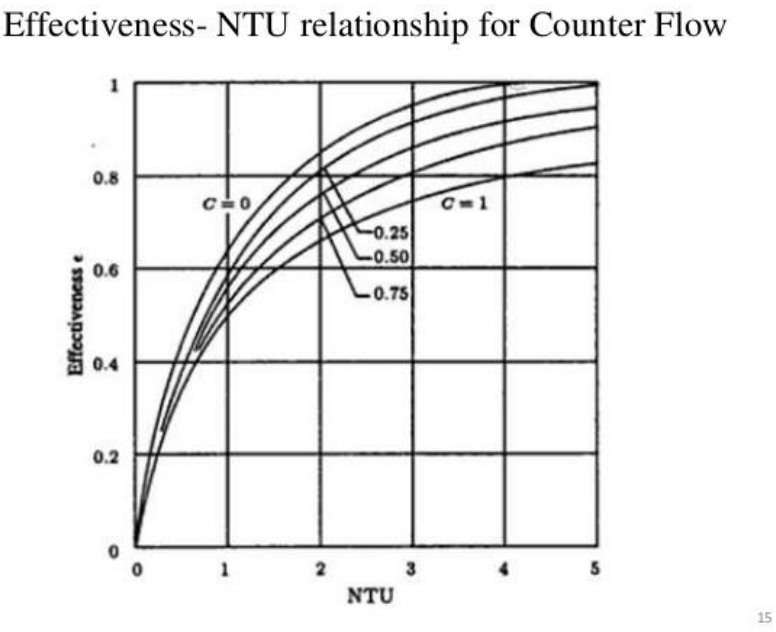

Figure 4-1 Effectiveness-NTU Relationship for Counter-flow Heat Exchanger

The above relation is considering constant properties, no axial conduction, no extended surfaces and no energy interaction with the environment. The following plot compares effectiveness computed using numerical model for various values of NTU with

effectiveness calculated analytical solution. The flow conditions are, balanced flow with no axial conduction and constant properties, but there is presence of extended surfaces to enhance heat transfer.

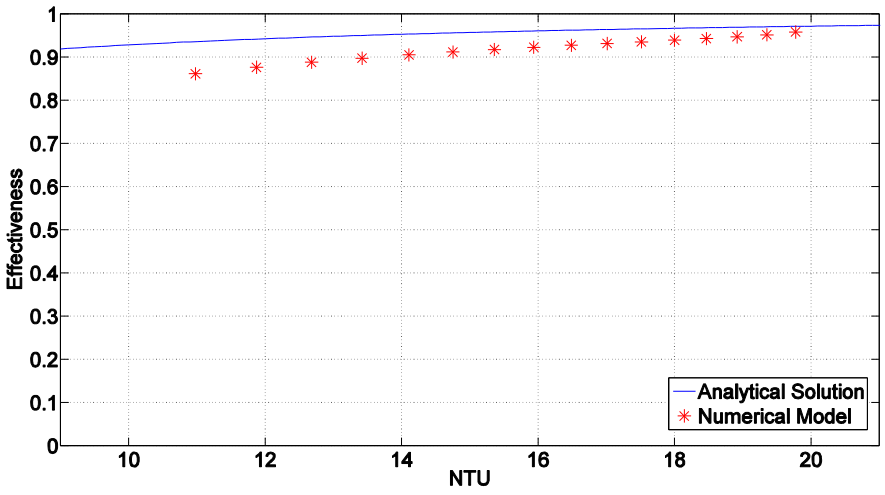

Figure 4-2 Comparison of Effectiveness Computed using Numerical Model and Analytical Solution

Figure 4-3 indicates nondimensional temperature profiles for a counter-flow heat exchanger with axial conduction and varying properties. There is a sharp drop in temperature of hot fluid immediately after it enters the heat exchanger and a corresponding temperature rise in cold fluid temperature at the cold end. These temperature “jumps” are associated with the transfer of heat from fluid into the metal at hot end, and out of the metal at cold end [22]. Thus axial conduction results in reduced effectiveness. The temperature “jump” effect mentioned by [22] can be seen in the following plot

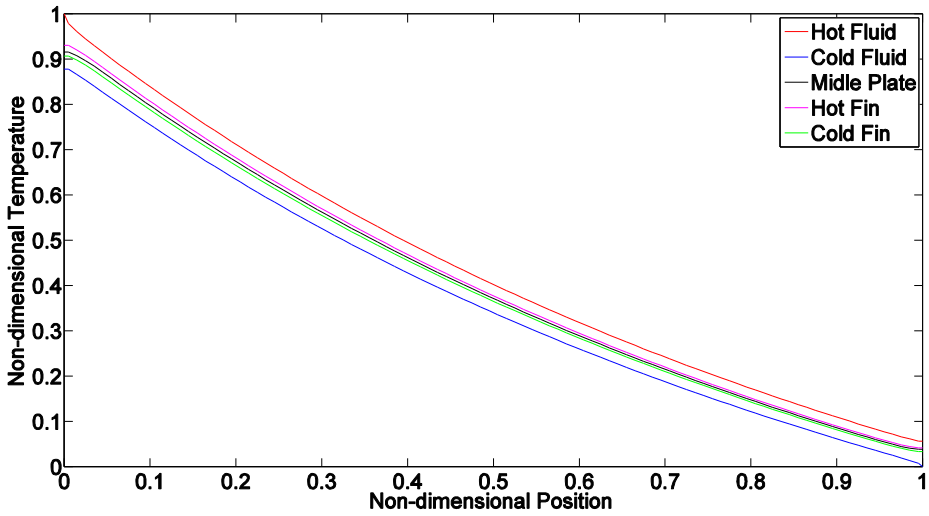

Figure 4-3 Non-dimensional Temperature vs. Non-dimensional Length for Counter-flow Heat Exchanger

The proceeding section demonstrates how the model can be utilized in context of a particular application.

4.2 Example Heat Exchanger Calculation

Numerical model presented in the thesis may be used to perform a detailed analysis of an arbitrary plate-fin heat exchanger. A specific example is presented in this section to demonstrate utility of the solver. The numerical model will be used to predict performance of a recuperator proposed to be a part of a solid oxide fuel cell - gas turbine hybrid system. The heat exchanger core will be analyzed according to boundary values dictated by steady state system cycle, the objective being thermal efficiency of 58%. The temperature and pressure of fluid at hot side inlet will be equal to that of the hot gases at turbine outlet. The state of fluid at inlet of cold side will be equal to that of the compressed air supplied by compressor. Compressed air will be supplied to solid oxide fuel cell stack, and hence should be preheated to a particular temperature before it enters

the cathode side of fuel cell. This target value is set as the design criteria for recuperator and sizing of heat exchanger is finalized depending on its performance analysis. The recuperator chosen is a plate fin heat exchanger with counter-flow configuration.

4.2.1 Boundary Conditions

1) Fluid Channels:

The temperatures at inlet of hot fluid and cold fluid channels and, the pressures at inlet and outlet of these channels are specified to the solver. Solver predicts temperature at the outlets of fluid channels. The fluid channels which are in contact with side wall are considered to have an adiabatic boundary condition at the side wall. It signifies that, heat transfer to the surroundings is neglected.

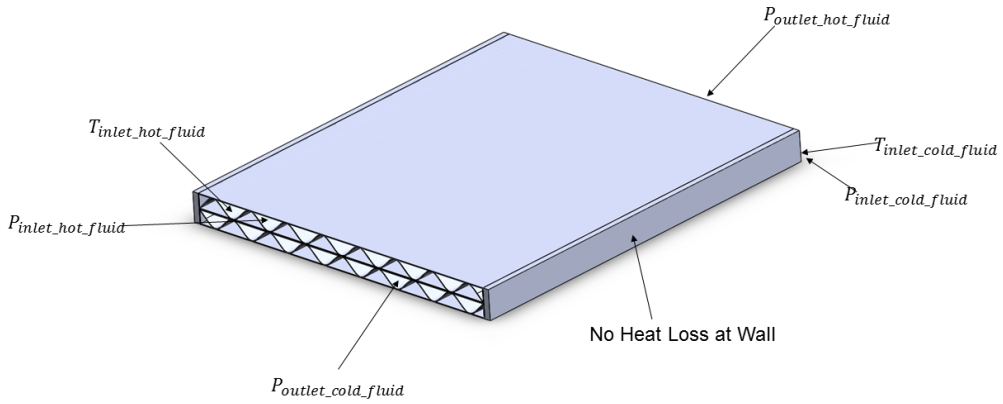

Figure 4-4 Boundary Conditions for Heat Exchanger Core Unit Module

2) Middle Plate and Fins:

The middle plate and fins are specified with an adiabatic boundary condition at inlet and outlet walls. Middle plate is specified with an adiabatic boundary condition at

side walls, which again signifies that heat interaction with surroundings is neglected and the setup is considered to be perfectly insulated.

4.2.2 Problem Setup

Consider the following hybrid system cycle.

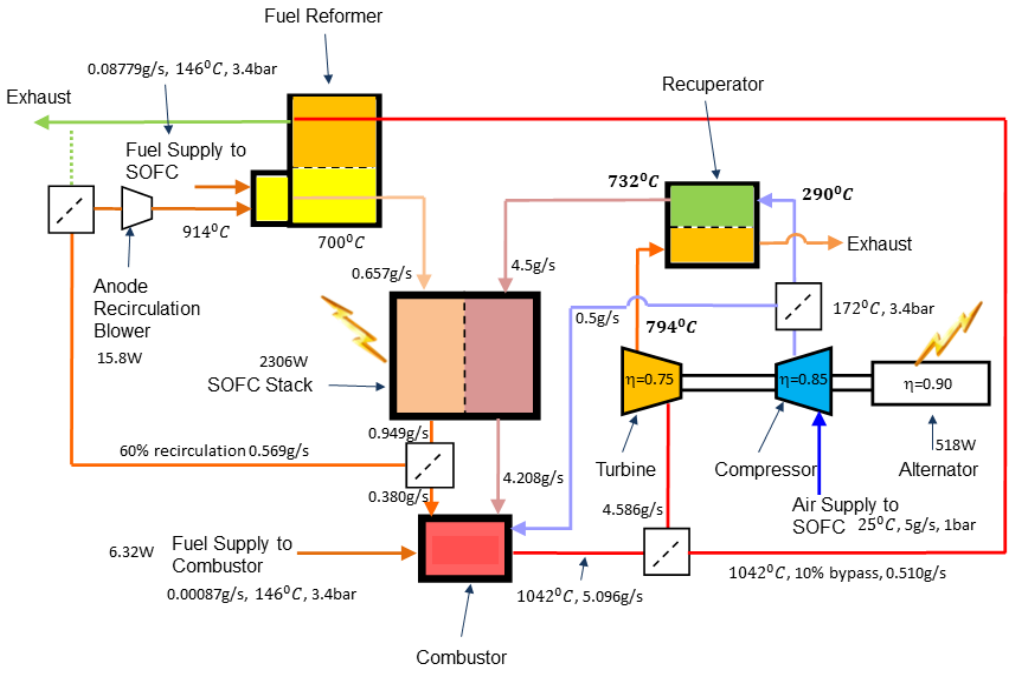

Figure 4-5 Hybrid Solid Oxide Fuel Cell-Gas Turbine Cycle Diagram

The system is designed with an objective to achieve 58% overall efficiency. According to the requirement for integration with hybrid system, temperature of hot fluid at inlet will be 1067 K and that of cold fluid will be 563K. The air supplied to fuel cell stack has to be at a temperature of 1005K. This is the value up to which cold fluid temperature has to be raised.

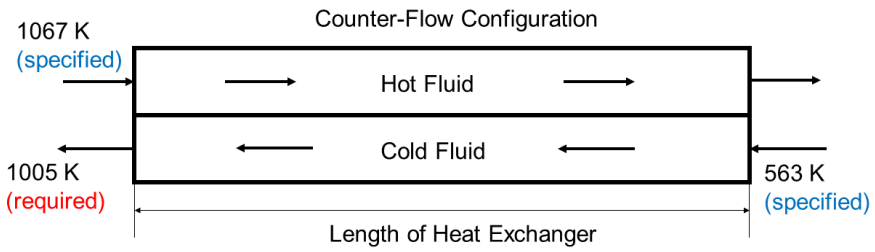

Figure 4-6 Channel Schematic

4.2.3 Results

The simulation were run for three cases of heat exchanger fin configurations. The three cases are listed as follows.

Case 1:

Hot Fluid: $T_{inlet} = 1067\ K$, temperature at inlet $P_{inlet} = 3.4 \times 10^5\ Pa$, pressure at inlet	Cold Fluid: $T_{inlet} = 563\ K$, temperature at inlet $P_{inlet} = 3.4 \times 10^5\ Pa$, pressure at inlet
Middle Plate: Material : Inconel 600 Thickness = $1.905\ mm$ Thermal Conductivity = $26.1\ W/(mK)$	Fins: Material : Fe-Cr Alloy Thickness = $0.1016\ mm$ Thermal Conductivity = $16\ W/(mK)$
Width of Heat Exchanger = $45\ mm$	Number of Channels per side = 15
Width of Channel = $6.42\ mm$ Height of Channel = $1.8\ mm$ Hydraulic Diameter = $1.677\ mm$ Heat Transfer Area = $1264\ m^2/m^3$	

Figure 4-7 Problem Setup Case 1

Case 2:

Hot Fluid: $T_{inlet} = 1067\ K$, temperature at inlet $P_{inlet} = 3.4 \times 10^5\ Pa$, pressure at inlet	Cold Fluid: $T_{inlet} = 563\ K$, temperature at inlet $P_{inlet} = 3.4 \times 10^5\ Pa$, pressure at inlet
Middle Plate: Material : Inconel 600 Thickness = $1.905\ mm$ Thermal Conductivity = $26.1\ W/(mK)$	Fins: Material : Fe-Cr Alloy Thickness = $0.1016\ mm$ Thermal Conductivity = $16\ W/(mK)$
Width of Heat Exchanger = $45\ mm$	Number of Channels per side = 31
Width of Channel = $3\ mm$ Height of Channel = $1.8\ mm$ Hydraulic Diameter = $1.405\ mm$ Heat Transfer Area = $1385\ m^2/m^3$	

Figure 4-8 Problem Setup Case 2

Case 3:

Hot Fluid: $T_{inlet} = 1067\ K$, temperature at inlet $P_{inlet} = 3.4 \times 10^5\ Pa$, pressure at inlet	Cold Fluid: $T_{inlet} = 563\ K$, temperature at inlet $P_{inlet} = 3.4 \times 10^5\ Pa$, pressure at inlet
Middle Plate: Material : Inconel 600 Thickness = $1.905\ mm$ Thermal Conductivity = $26.1\ W/(mK)$	Fins: Material : Fe-Cr Alloy Thickness = $0.1016\ mm$ Thermal Conductivity = $16\ W/(mK)$
Width of Heat Exchanger = $45\ mm$	Number of Channels per side = 51
Width of Channel = $1.8\ mm$ Height of Channel = $1.8\ mm$ Hydraulic Diameter = $1.112\ mm$ Heat Transfer Area = $1870\ m^2/m^3$	

Figure 4-9 Problem Setup Case 3

The number of fins on each side were increased for increasing total heat transfer area per unit volume. The changes in temperature at cold channel outlet, effectiveness, heat transfer coefficients and pressure drop depending on number of fins and hence compactness were studied.

The requirement for cold fluid temperature at outlet is 1005 K. The numerical model was used to perform simulations for various lengths. The length of recuperator which delivers target output temperature was selected with a consideration for pressure drop. Compactness is a major concern for distributed power generation systems. The compromise between the sizing, effectiveness and pressure drop in heat exchanger will be an important consideration. The solver will help in approximating fluid and thermal characteristics of flow and hence narrow down to an optimum design. The pressure drops across various length for above values of compactness are shown in the following plot

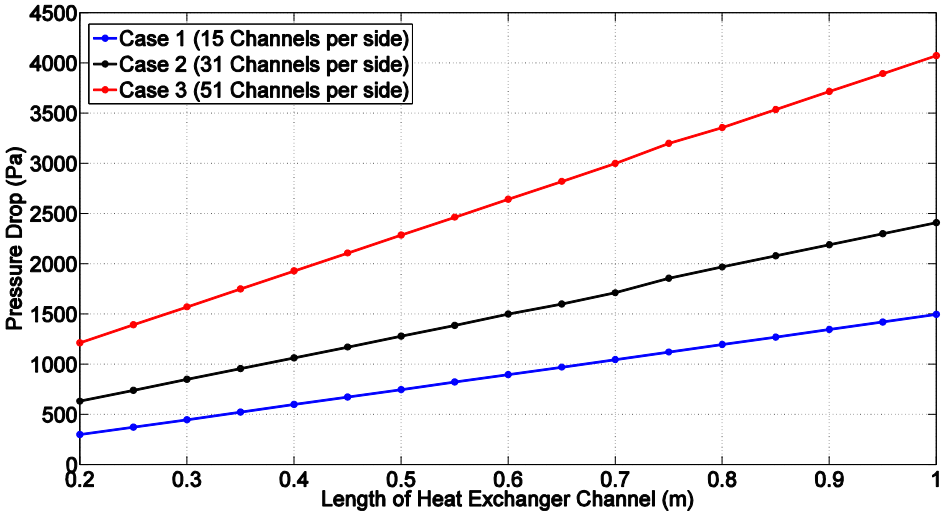

Figure 4-10 Pressure Drop across Length of Heat Exchanger Channel

Following are the plots for effectiveness for three different cases. The effectiveness computed by solver is compared to effectiveness calculated by analytical method.

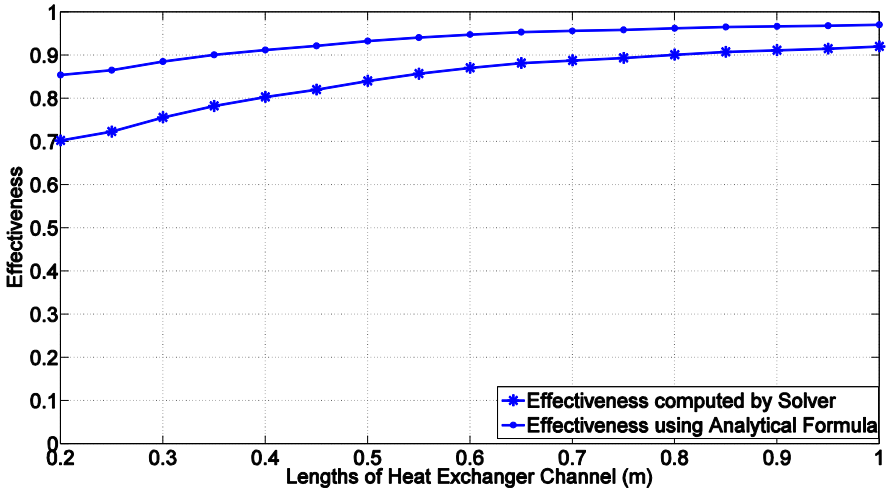

Figure 4-11 Effectiveness for Case 1 (15 Channels per side)

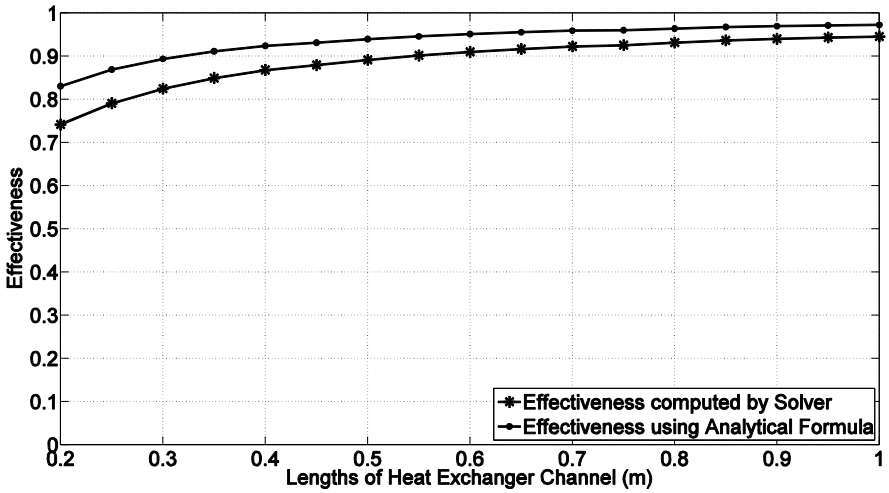

Figure 4-12 Effectiveness for Case 2 (31 Channels per side)

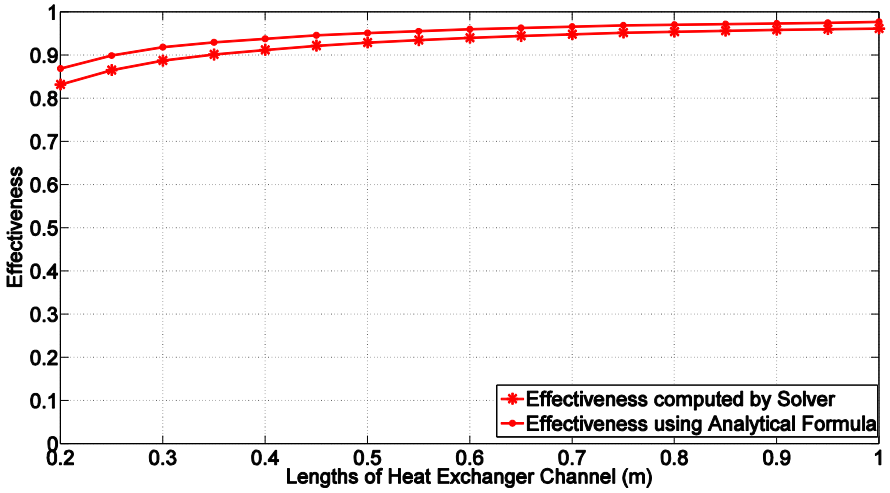

Figure 4-13 Effectiveness for Case 3 (51 Channels per side)

The following plot shows temperature at cold channels outlet for various lengths of heat exchanger considering three cases.

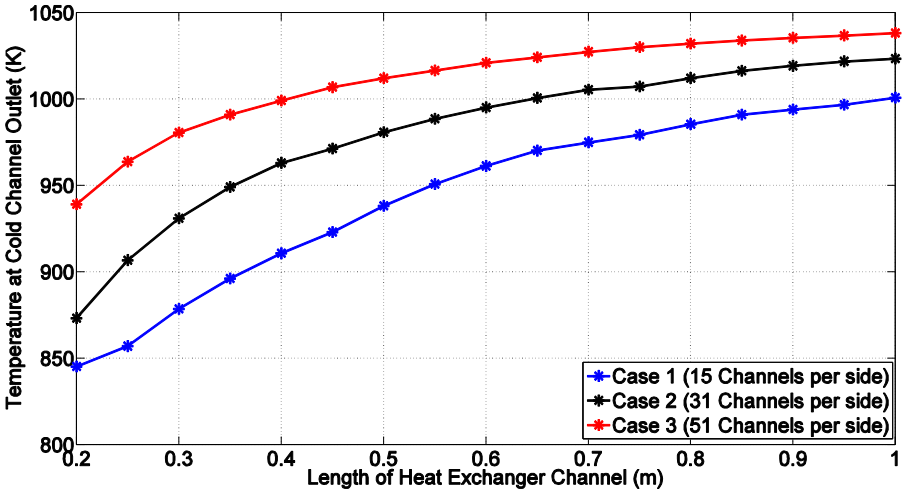

Figure 4-14 Temperature at Cold Channel Outlet vs. Lengths of Heat Exchanger

The following plot shows effectiveness computed by solver for various lengths of heat exchanger considering three cases.

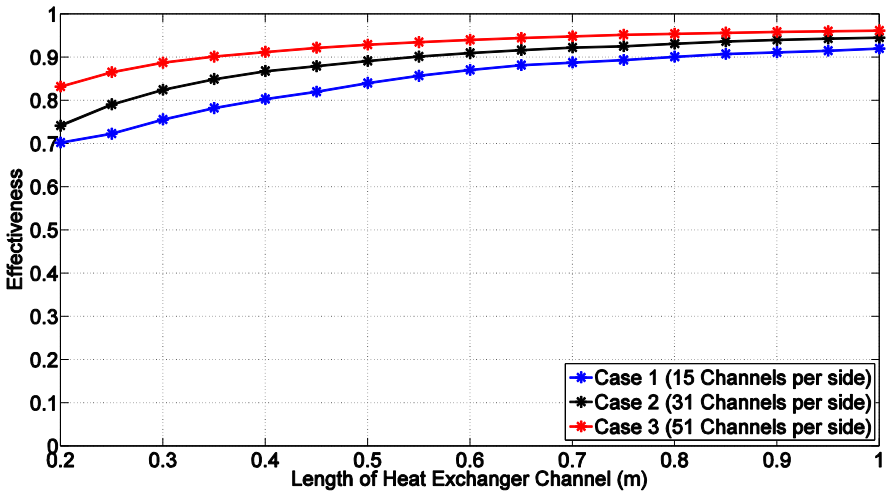

Figure 4-15 Effectiveness vs. Lengths of Heat Exchanger

As we can observe from the plots, target temperature of 1005 K is attained at shorter length when heat transfer area is $1870\ m^2/m^3$. For heat transfer area of $1385\ m^2/m^3$, required value is attained at farther length, and for heat transfer area of $1264\ m^2/m^3$, length where heat exchanger delivers 1005 K is the farthest. Considering the compromise between temperature requirement, pressure drop, compactness and cost effectiveness, we consider the Case 2 for further simulations.

The heat exchanger width is fixed at 0.045 m. Simulations were run for various lengths of heat exchanger. Length of 0.7 m resulted in an effectiveness of 92.25 % and the average cold fluid outlet temperature of 1005 K. The pressure drop across both channels was considered to be 1700 Pa for given length. The following plot show heat transfer coefficient for 0.700 m length of heat exchanger considering three cases.

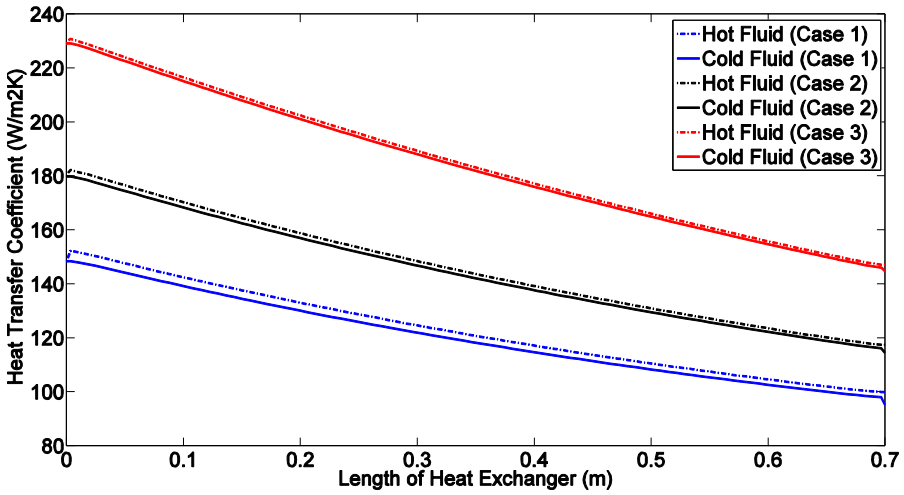

Figure 4-16 Heat Transfer Coefficient vs. Length of Heat Exchanger

Following is the plots for temperature of fluids vs. length of heat exchanger for 0.700 m considering Case 2.

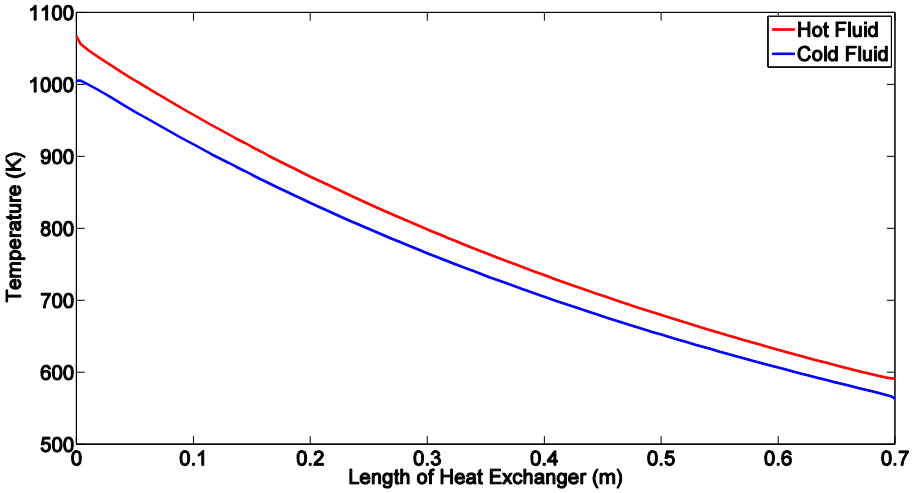

Figure 4-17 Fluid Temperature vs. Length of Heat Exchanger (0.700 m)

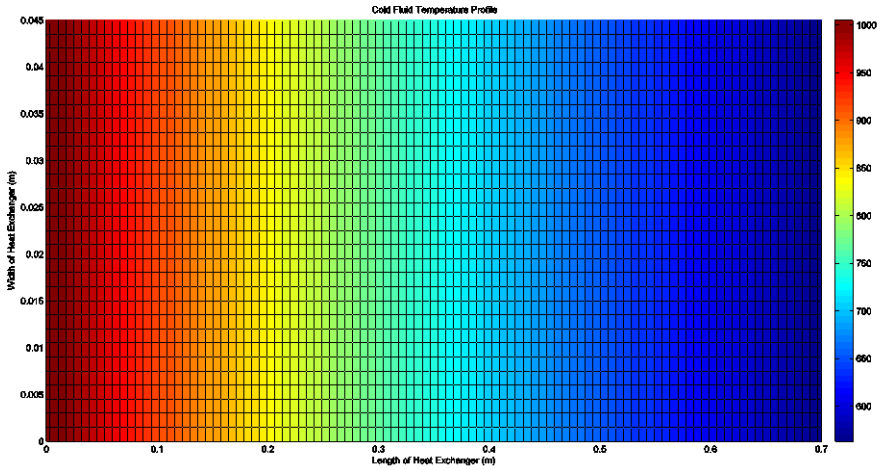

Figure 4-18 Cold fluid temperature across flow field

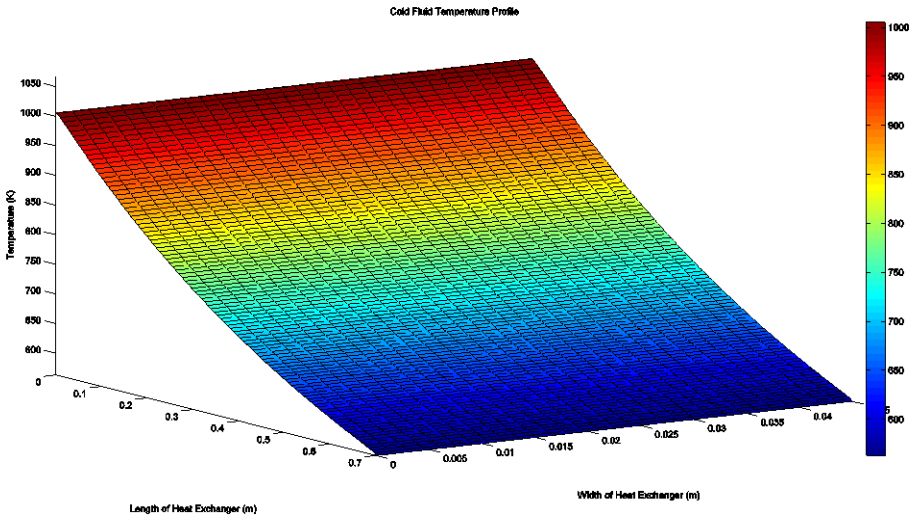

Figure 4-19 Cold fluid temperature across flow field

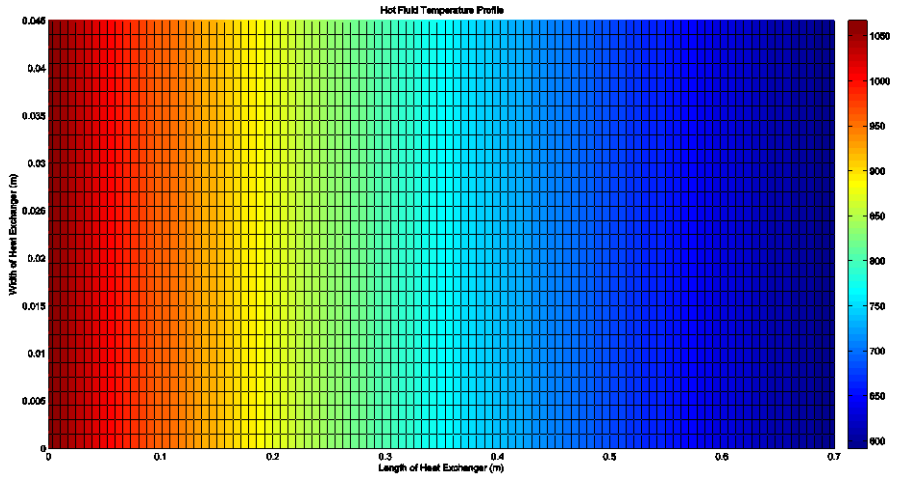

Figure 4-20 Hot fluid temperature across flow field

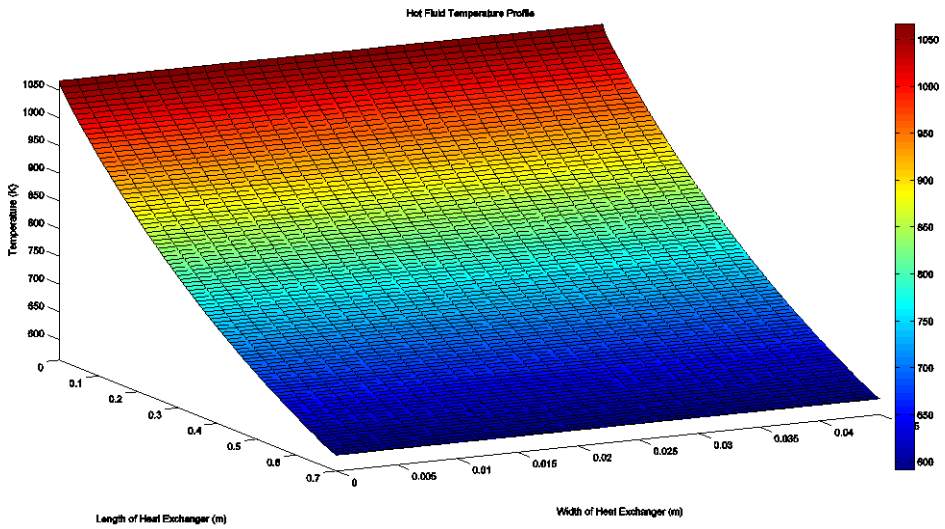

Figure 4-21 Hot fluid temperature across flow field

As it can be observed from the plots, temperature along width is constant. The adiabatic condition at walls is reason for the later. The following plots show temperature and effectiveness for three cases without axial conduction, computed by the solver.

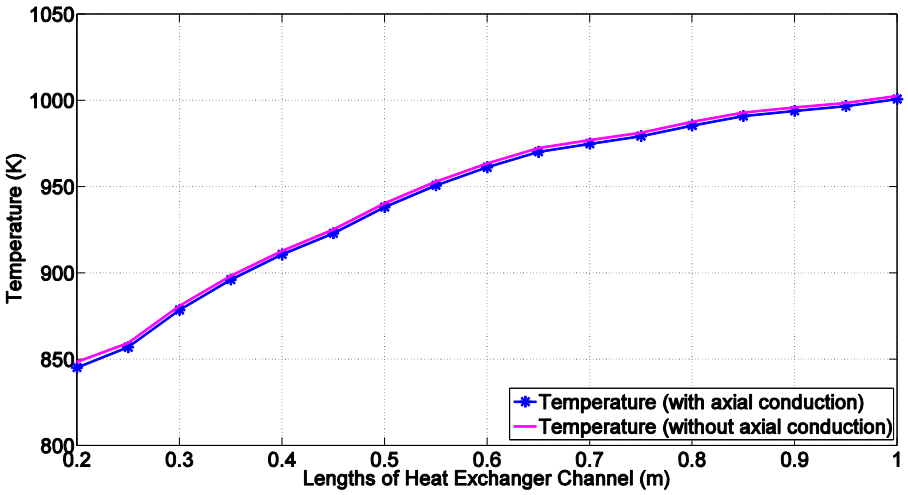

Figure 4-22 Temperature vs. Lengths of Heat Exchanger for 'With' and 'Without' Axial Conduction (Case 1)

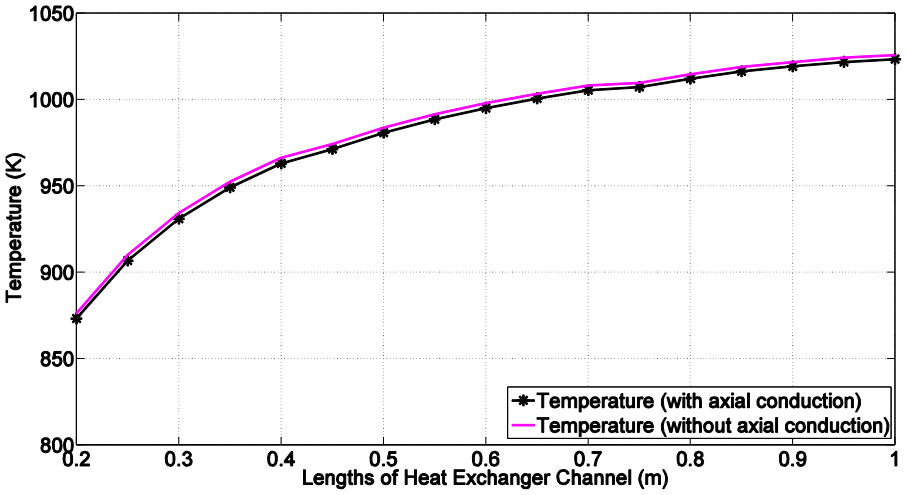

Figure 4-23 Temperature vs. Lengths of Heat Exchanger for 'With' and 'Without' Axial Conduction (Case 2)

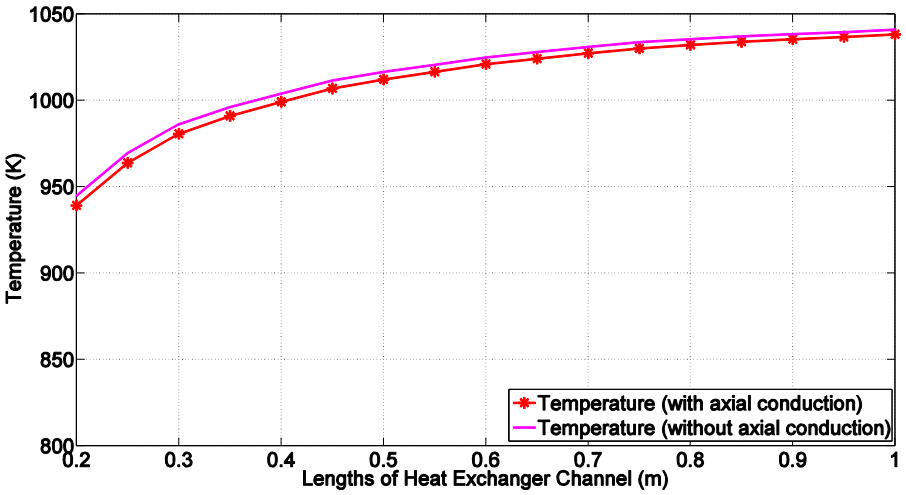

Figure 4-24 Temperature vs. Lengths of Heat Exchanger for 'With' and 'Without' Axial Conduction (Case 3)

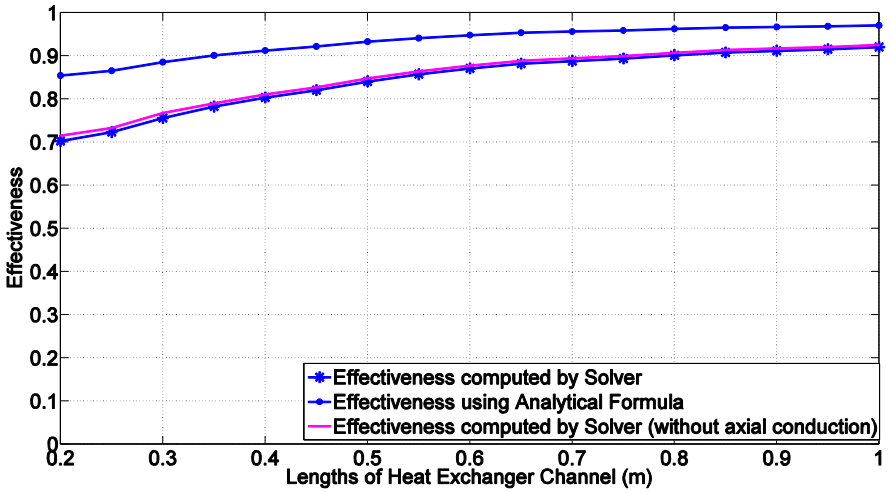

Figure 4-25 Effectiveness vs. Lengths of Heat Exchanger for 'With' and 'Without' Axial Conduction (Case 1)

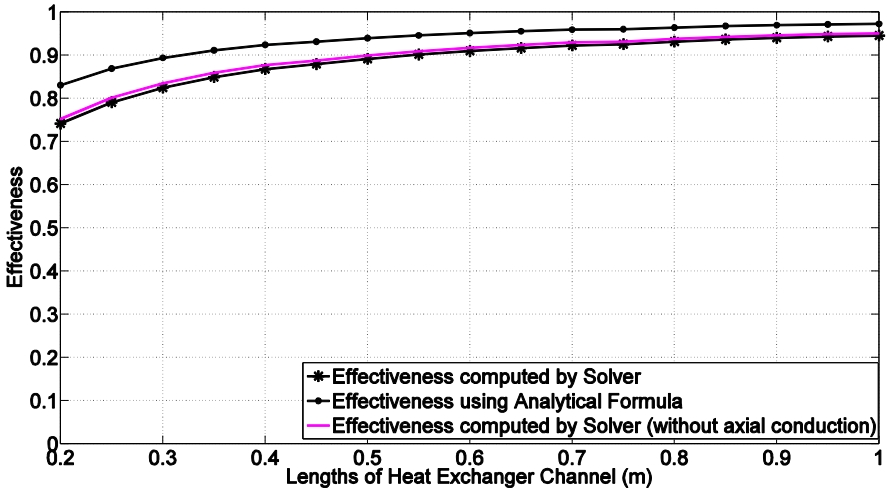

Figure 4-26 Effectiveness vs. Lengths of Heat Exchanger for 'With' and 'Without' Axial Conduction (Case 2)

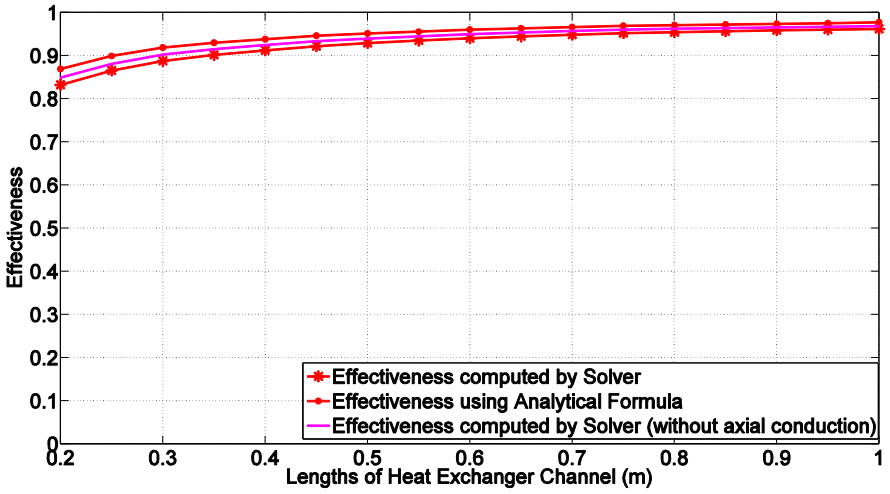

Figure 4-27 Effectiveness vs. Lengths of Heat Exchanger for 'With' and 'Without' Axial Conduction (Case 3)

Therefore we can observe that axial conduction causes degradation of performance of heat exchanger.

Chapter 5

CONCLUSIONS

The thesis presents numerical model of a plate-fin type heat exchanger which uses finite volume method for discretization and solves for mass flow rate and temperature of fluid, as well as temperatures of solid structure. The solver uses temperatures at inlet, and pressures at inlet and outlet of heat exchanger channels as boundary conditions to solve momentum and energy equations across the flow field. The property variations of fluid according to temperature and axial conduction in solid structure are modeled in the solver. The energy transport through fluid is modeled using advection-diffusion equation and the energy transport through solid structure is modeled using diffusion equation.

The numerical model will act as a foundation for simulation of more complex fluid flows, for instance multi-phase flows and reacting mixtures. Features in the solver can be changed according to type of fluid required to be handled by the system. The solver is user-friendly and gives complete control to user for changing or optimizing methods according to his needs. For example, a different approach for predicting the face values can be used with a few simple modifications.

The model will prove useful to approximate the fluid properties at heat exchanger outlet depending on given inlet temperature and pressure drop. The solver can be used as an effective tool to predict performance of a heat transfer device and narrow down on design options when the heat exchanger needs to be integrated with other fluid flow devices upstream or downstream. The model is developed as a callable sub-routine, as well as a stand-alone program so that it can be easily integrated into more complex, system level simulations.

Chapter 6

SCOPE FOR FUTURE WORK

The future objectives are listed as follows:

1) The method for approximating face values in advection-diffusion equation can be replaced with higher order methods to check whether they lead to increased accuracy of approximation. An increased accuracy of result can be acceptable, even if the procedure becomes computationally expensive by a small margin.

2) The heat losses to environment will be modelled to make the simulation more realistic. One approach can be that, the core can be considered to be in contact with the casing and the casing is exposed to surroundings. Another approach can be that, the core is directly exchanging heat with surroundings.

3) The solver can be upgraded to simulate multiple units of heat exchanger core and hence simulate the complete stack instead of single module. The model can first solve for mass flow rate and then consider required number of stacks to simulate target mass flow rate for the device or a value closer to it.

4) Modules can be developed and the momentum and energy equations can be upgraded to handle multi-phase fluid flows. This modification can be of great use in HVAC domain.

5) Upgradations in formulations for momentum and energy equations can be made to simulate reacting mixture flows. The methods to calculate the fluid properties as a

function of temperature and pressure have to be revised to account for mixture of species.

The modifications and upgradations in the solver are targeted towards getting an even accurate approximation of fluid behavior.

APPENDIX A

Tables

Pressure drop values for three cases of fin configurations, for various lengths of heat exchanger.

Table A-1 Pressure Drop for Various Lengths of Heat Exchanger

Length of Heat Exchanger Channel (m)	Pressure Drop (Pa)		
	Case 1 15 Channels	Case 2 31 Channels	Case 3 51 Channels
0.200	300	632	1214
0.250	374	740	1393
0.300	448	850	1572
0.350	523	956	1750
0.400	600	1064	1929
0.450	673	1172	2108
0.500	748	1280	2286
0.550	823	1388	2465
0.600	897	1500	2644
0.650	972	1600	2822
0.700	1047	1712	3001
0.750	1122	1858	3108
0.800	1197	1969	3358
0.850	1271	2079	3537
0.900	1346	2190	3716
0.950	1421	2300	3895
1.000	1496	2411	4073

Temperature and effectiveness values for various lengths of heat exchanger. The temperature specified is at cold outlet for given length and effectiveness is based on enthalpy gain of cold fluid.

Case 1 (15 channels):

Table A-2 Temperature and Effectiveness Values for Various Lengths of Heat Exchanger (Case 1)

Length of Heat Exchanger Channel (m)	Temperature at Cold Outlet (K)	Effectiveness	Effectiveness using Analytical Formula	Without Axial Conduction	
				Temperature at Cold Outlet (K)	Effectiveness
0.200	845.26	0.7024	0.8540	848.57	0.7153
0.250	856.95	0.7228	0.8651	859.45	0.7324
0.300	878.52	0.7559	0.8854	880.92	0.7674
0.350	896.10	0.7820	0.9005	898.39	0.7900
0.400	910.69	0.8029	0.9122	912.89	0.8103
0.450	923.01	0.8202	0.9215	925.11	0.8270
0.500	938.16	0.8404	0.9324	940.35	0.8473
0.550	950.71	0.8568	0.9410	952.97	0.8637
0.600	961.23	0.8703	0.9478	963.53	0.8771
0.650	970.13	0.8816	0.9533	972.46	0.8882

0.700	974.90	0.8878	0.9561	977.10	0.8940
0.750	979.24	0.8934	0.9586	981.33	0.8992
0.800	985.47	0.9011	0.9622	987.57	0.9068
0.850	990.92	0.9077	0.9653	993.03	0.9134
0.900	993.88	0.9115	0.9668	995.89	0.9169
0.950	996.64	0.9150	0.9682	998.56	0.9201
1.000	1000.75	0.9200	0.9705	1002.67	0.9250

Case 2 (31 channels):

Table A-3 Temperature and Effectiveness Values for Various Lengths of Heat Exchanger (Case 2)

Length of Heat Exchanger Channel (m)	Temperature at Cold Outlet (K)	Effectiveness	Effectiveness using Analytical Formula	Without Axial Conduction	
				Temperature at Cold Outlet (K)	Effectiveness
0.200	873.24	0.7413	0.8303	876.22	0.7522
0.250	906.75	0.7907	0.8687	909.96	0.8014
0.300	930.96	0.8246	0.8938	934.26	0.8350
0.350	949.08	0.8493	0.9113	952.40	0.8592
0.400	963.07	0.8679	0.9241	966.37	0.8774
0.450	971.32	0.8791	0.9311	974.35	0.8876
0.500	980.77	0.8913	0.9392	983.76	0.8995
0.550	988.56	0.9012	0.9457	991.50	0.9091
0.600	995.08	0.9095	0.9509	997.97	0.9171
0.650	1000.63	0.9165	0.9553	1003.45	0.9238
0.700	1005.39	0.9225	0.9590	1008.16	0.9295
0.750	1007.2	0.9252	0.9601	1009.71	0.9315

0.800	1012.12	0.9311	0.9640	1014.68	0.9375
0.850	1016.35	0.9362	0.9673	1018.95	0.9425
0.900	1019.2	0.9397	0.9694	1021.75	0.9459
0.950	1021.76	0.9429	0.9712	1024.25	0.9489
1.000	1023.40	0.9451	0.9723	1025.78	0.9508

Case 3 (51 channels):

Table A-4 Temperature and Effectiveness Values for Various Lengths of Heat Exchanger (Case 3)

Length of Heat Exchanger Channel (m)	Temperature at Cold Outlet (K)	Effectiveness	Effectiveness using Analytical Formula	Without Axial Conduction	
				Temperature at Cold Outlet (K)	Effectiveness
0.200	939.15	0.8321	0.8689	944.72	0.8487
0.250	963.78	0.8652	0.8990	969.44	0.8810
0.300	980.60	0.8873	0.9184	986.19	0.9022
0.350	990.96	0.9012	0.9294	996.11	0.9146
0.400	999.11	0.9121	0.9378	1003.89	0.9242
0.450	1006.82	0.9219	0.9460	1011.49	0.9334
0.500	1012.01	0.9288	0.9511	1016.44	0.9394
0.550	1016.48	0.9346	0.9554	1020.61	0.9445
0.600	1020.91	0.9401	0.9599	1024.94	0.9496
0.650	1024.09	0.9443	0.9628	1027.91	0.9532
0.700	1027.32	0.9484	0.9661	1031.02	0.9569
0.750	1030.05	0.9518	0.9688	1033.63	0.9599

0.800	1032.06	0.9544	0.9706	1035.43	0.9620
0.850	1033.83	0.9566	0.9722	1037	0.9638
0.900	1035.38	0.9586	0.9737	1038.36	0.9653
0.950	1036.73	0.9603	0.9750	1039.53	0.9666
1.000	1038.17	0.9618	0.9768	1040.87	0.9679

REFERENCES

[1] Hybrid Gas Turbine fuel Cell Systems Report, Jack Brouwer

[2] Dustin McLarty, Jack Brouwer, Scott Samuelsen, “Fuel cell-gas turbine hybrid system design part 1: Steady state performance”, Journal of Power Sources 257 (2014) 412-420

[3] Jeongpill Ki, Daejong Kim, Srikanth Honavara-Prasad, “Dynamic Modeling of a Compact Heat Exchange Reformer for high Temperature Fuel Cell Systems” Journal of Fuel Cell Science and Technology, February 2012, Vol. 9, 011013-1

[4] ALPEMA, The Standards for the Brazed Aluminium Plate Fin Heat Exchanger Manufactures' Association (http://www.alpema.org/)

[5] Kays, W.M. and London, A.L. Compact Heat exchangers, McGraw-Hill, New York (1984)

[6] Kern, D.Q., Kraus, A.D. Extended Surface Heat Transfer, McGraw-Hill, New York (1972)

[7] Frass, A.P., Heat Exchanger Design, 2nd ed., Wiley-Inter science (1989)

[8] Ozisik, M.N., Heat Transfer-A Basic Approach, McGraw-Hill (1985)

[9] Incropera, F.P., Dewitt, D.P. Fundamentals of Heat Transfer 2nd ed. John Wiley, New York, 1985

[10] Shah, R.K., Dusan,P., Sekulic,D.P. Fundamentals of Heat Exchanger Design, John Wiley & Sons, (2003)

[11] Shah, R.K. Compact Heat Exchangers & Enhancement Technology, Begell House Publication, (1999)

[12] Applied Thermal Engineering (http://www.elsvier.com)

[13] Experimental Thermal and Fluid Science (http://www.elsevier.com)

[14] Journal of Heat Transfer (http://www.asme.org)

[15] International Journal of Heat and Mass transfer (http://www.elsevier.com)

[16] Heat Transfer Engineering (http://www.tandf.co.uk./journals/titles/01457632.asp)

[17] International Journal of Heat Exchangers

[18] Kays, W.M. and London, A.L. “Description of Test equipment and method of Analysis for basic Heat transfer and flow friction test of high rating heat exchanger surfaces Technical Report No. 2”, Department of Mechanical Engineering, Stanford University (1948)

[19] Kroeger PG. “Performance deterioration in high effectiveness heat exchanger due to axial heat conduction effects”. Advances in cryogenic engineering, vol. 31. Plenum; 1967. p. 363–72.

[20] Narayanan SP, Venkatarathnam G. “Performance degradation due to longitudinal heat conduction in very high NTU counterflow heat exchangers”. Cryogenics 1998; 38:927–30.

[21] Chowdhury K, Sarangi S. “Performance of cryogenic heat exchangers with heat leak from the surroundings”. Adv Cryog Eng 1984; 29:273–80.

[22] G.F. Nellis, “A heat exchanger model that includes axial conduction, parasitic heat loads, and property variations”, Elsevier Cryogenics 43 (2003) 523–538

[23] Shah, R.K. Classification of heat exchangers, Heat Exchangers, Thermal-Hydraulic Fundamentals and Design, by S. Kakac, A.E. Bergles, F. Mayinger, Hemisphere Publication (1980) 9-46

[24] Experimental Studies on Plate Fin Heat Exchangers, by Sidramappa Alur, Mechanical Engineering Department, National Institute of Technology, Rourkela, India

[25] Experimental and Computational Studies on Plate Fin Heat Exchangers, by Indranil Ghosh, Cryogenic Engineering Centre, Indian Institute of Technology, Kharagpur, India

BIOGRAPHICAL INFORMATION

Ajit Desai received Bachelors in Mechanical Engineering Degree from University of Mumbai. Thereafter he joined University of Texas at Arlington to pursue Masters of Science in Mechanical Engineering. His specialization is in thermal engineering and fluid sciences. During the course of graduate degree, he completed an internship at Siemens Corporate Technology.

The focus of Ajit Desai's research is based on hybrid power generation systems. He works on computational modeling and analysis of thermal engineering and fluid flow equipment used in power generation systems.